REFERENCES

1. Nagasawa T. Microenvironmental niches in the bone marrow required for B-cell development. Nat Rev Immunol. 2006;6:107-116.
2. Maddaly R, Pai G, Balaji S et al. Receptors and signaling mechanisms for B-lymphocyte activation, proliferation and differentiation--insights from both in vivo and in vitro approaches. FEBS Lett. 2010;584:4883-4894.
3. Tanaka T, Yoshida N, Kishimoto T et al. Defective adipocyte differentiation in mice lacking the C/EBPbeta and/or C/EBPdelta gene. EMBO J. 1997;16:7432-7443.
4. Ramji DP, Foka P. CCAAT/enhancer-binding proteins: structure, function and regulation. Biochem J. 2002;365:561-575.
5. Nerlov C. The C/EBP family of transcription factors: a paradigm for interaction between gene expression and proliferation control. Trends Cell Biol. 2007;17:318-324.
6. Hirai H, Zhang P, Dayaram T et al. C/EBPbeta is required for 'emergency' granulopoiesis. Nat Immunol. 2006;7:732-739.
7. Akagi T, Saitoh T, O'Kelly J et al. Impaired response to GM-CSF and G-CSF, and enhanced apoptosis in C/EBPbeta-deficient hematopoietic cells. Blood. 2008;111:2999-3004.
8. Satake S, Hirai H, Hayashi Y et al. C/EBPbeta is involved in the amplification of early granulocyte precursors during candidemia-induced "emergency" granulopoiesis. J Immunol. 2012;189:4546-4555.
9. Bianco P, Riminucci M, Gronthos S et al. Bone marrow stromal stem cells: nature, biology, and potential applications. Stem Cells. 2001;19:180-192.
10. Nagasawa T, Omatsu Y, Sugiyama T. Control of hematopoietic stem cells by the bone marrow stromal niche: the role of reticular cells. Trends Immunol. 2011;32:315-320.
11. Mercier FE, Ragu C, Scadden DT. The bone marrow at the crossroads of blood and immunity. Nat Rev Immunol. 2012;12:49-60.
12. Screpanti I, Romani L, Musiani P et al. Lymphoproliferative disorder and imbalanced T-helper response in C/EBP beta-deficient mice. EMBO J. 1995;14:1932-1941.
13. Okabe M, Ikawa M, Kominami K et al. 'Green mice' as a source of ubiquitous green cells. FEBS Lett. 1997;407:313-319.
14. Wang L, Zhao Y, Liu Y et al. IFN-gamma and TNF-alpha Synergistically Induce Mesenchymal Stem Cell Impairment and Tumorigenesis via NFkappaB Signaling. Stem Cells. 2013;31:1383-1395.
15. Miura M, Chen XD, Allen MR et al. A crucial role of caspase-3 in osteogenic differentiation of bone marrow stromal stem cells. J Clin Invest. 2004;114:1704-1713.
16. Miura Y, Miura M, Gronthos S et al. Defective osteogenesis of the stromal stem cells predisposes CD18-null mice to osteoporosis. Proc Natl Acad Sci U S A. 2005;102:14022-14027.
17. Shi S, Gronthos S, Chen S et al. Bone formation by human postnatal bone marrow stromal stem cells is enhanced by telomerase expression. Nat Biotechnol. 2002;20:587-591.
18. Miura M, Miura Y, Sonoyama W et al. Bone marrow-derived mesenchymal stem cells for regenerative medicine in craniofacial region. Oral Dis. 2006;12:514-522.
19. Miura Y, Gao Z, Miura M et al. Mesenchymal stem cell-organized bone marrow elements: an alternative hematopoietic progenitor resource. Stem Cells. 2006;24:2428-2436.

20. Yamaza T, Miura Y, Akiyama K et al. Mesenchymal stem cell-mediated ectopic hematopoiesis alleviates aging-related phenotype in immunocompromised mice. Blood. 2009;113:2595-2604.
21. Yokota A, Kimura S, Masuda S et al. INNO-406, a novel BCR-ABL/Lyn dual tyrosine kinase inhibitor, suppresses the growth of Ph+ leukemia cells in the central nervous system, and cyclosporine A augments its in vivo activity. Blood. 2007;109:306-314.
22. Kawada H, Ando K, Tsuji T et al. Rapid ex vivo expansion of human umbilical cord hematopoietic progenitors using a novel culture system. Exp Hematol. 1999;27:904-915.
23. Hardy RR, Shinton SA. Characterization of B lymphopoiesis in mouse bone marrow and spleen. Methods Mol Biol. 2004;271:1-24.
24. Chen X, Liu W, Ambrosino C et al. Impaired generation of bone marrow B lymphocytes in mice deficient in C/EBPbeta. Blood. 1997;90:156-164.
25. Tokoyoda K, Egawa T, Sugiyama T et al. Cellular niches controlling B lymphocyte behavior within bone marrow during development. Immunity. 2004;20:707-718.
26. Nagasawa T, Hirota S, Tachibana K et al. Defects of B-cell lymphopoiesis and bone-marrow myelopoiesis in mice lacking the CXC chemokine PBSF/SDF-1. Nature. 1996;382:635-638.
27. Egawa T, Kawabata K, Kawamoto H et al. The earliest stages of B cell development require a chemokine stromal cell-derived factor/pre-B cell growth-stimulating factor. Immunity. 2001;15:323-334.
28. Phinney DG, Prockop DJ. Concise review: mesenchymal stem/multipotent stromal cells: the state of transdifferentiation and modes of tissue repair--current views. Stem Cells. 2007;25:2896-2902.
29. Dominici M, Le Blanc K, Mueller I et al. Minimal criteria for defining multipotent mesenchymal stromal cells. The International Society for Cellular Therapy position statement. Cytotherapy. 2006;8:315-317.
30. Dias S, Silva H, Jr., Cumano A et al. Interleukin-7 is necessary to maintain the B cell potential in common lymphoid progenitors. J Exp Med. 2005;201:971-979.
31. Ishii T, Nishihara M, Ma F et al. Expression of stromal cell-derived factor-1/pre-B cell growth-stimulating factor receptor, CXC chemokine receptor 4, on CD34+ human bone marrow cells is a phenotypic alteration for committed lymphoid progenitors. J Immunol. 1999;163:3612-3620.
32. Kim KJ, Kim HH, Kim JH et al. Chemokine stromal cell-derived factor-1 induction by C/EBPbeta activation is associated with all-trans-retinoic acid-induced leukemic cell differentiation. J Leukoc Biol. 2007;82:1332-1339.
33. Calonge E, Alonso-Lobo JM, Escandon C et al. c/EBPbeta is a major regulatory element driving transcriptional activation of the CXCL12 promoter. J Mol Biol. 2010;396:463-472.
34. Friedenstein AJ, Chailakhyan RK, Latsinik NV et al. Stromal cells responsible for transferring the microenvironment of the hemopoietic tissues. Cloning in vitro and retransplantation in vivo. Transplantation. 1974;17:331-340.
35. Owen M, Friedenstein AJ. Stromal stem cells: marrow-derived osteogenic precursors. Ciba Found Symp. 1988;136:42-60.
36. Prockop DJ. Marrow stromal cells as stem cells for nonhematopoietic tissues. Science. 1997;276:71-74.
37. Pittenger MF, Mackay AM, Beck SC et al. Multilineage potential of adult human mesenchymal stem cells. Science. 1999;284:143-147.
38. Zhu J, Garrett R, Jung Y et al. Osteoblasts support B-lymphocyte commitment and differentiation from

hematopoietic stem cells. Blood. 2007;109:3706-3712.

39. Sugiyama T, Kohara H, Noda M et al. Maintenance of the hematopoietic stem cell pool by CXCL12-CXCR4 chemokine signaling in bone marrow stromal cell niches. Immunity. 2006;25:977-988.
40. Lane SW, Scadden DT, Gilliland DG. The leukemic stem cell niche: current concepts and therapeutic opportunities. Blood. 2009;114:1150-1157.
41. Carlesso N, Cardoso AA. Stem cell regulatory niches and their role in normal and malignant hematopoiesis. Curr Opin Hematol. 2010;17:281-286.
42. Raaijmakers MH, Mukherjee S, Guo S et al. Bone progenitor dysfunction induces myelodysplasia and secondary leukaemia. Nature. 2010;464:852-857.
43. Konopleva MY, Jordan CT. Leukemia stem cells and microenvironment: biology and therapeutic targeting. J Clin Oncol. 2011;29:591-599.
44. Iwamoto S, Mihara K, Downing JR et al. Mesenchymal cells regulate the response of acute lymphoblastic leukemia cells to asparaginase. J Clin Invest. 2007;117:1049-1057.
45. Nwabo Kamdje AH, Krampera M. Notch signaling in acute lymphoblastic leukemia: any role for stromal microenvironment? Blood. 2011;118:6506-6514.
46. Purizaca J, Meza I, Pelayo R. Early lymphoid development and microenvironmental cues in B-cell acute lymphoblastic leukemia. Arch Med Res. 2012;43:89-101.
47. Burger JA, Burkle A. The CXCR4 chemokine receptor in acute and chronic leukaemia: a marrow homing receptor and potential therapeutic target. Br J Haematol. 2007;137:288-296.
48. Mowafi F, Cagigi A, Matskova L et al. Chemokine CXCL12 enhances proliferation in pre-B-ALL via STAT5 activation. Pediatr Blood Cancer. 2008;50:812-817.
49. Teicher BA, Fricker SP. CXCL12 (SDF-1)/CXCR4 pathway in cancer. Clin Cancer Res. 2010;16:2927-2931.
50. Block GJ, Ohkouchi S, Fung F et al. Multipotent stromal cells are activated to reduce apoptosis in part by upregulation and secretion of stanniocalcin-1. Stem Cells. 2009;27:670-681.

See www.StemCells.com for supporting information available online.

Figure 1. The level of precursor B-cells is reduced in the bone marrow of C/EBPβ-KO mice. The percentage of $B220^+$ B-cells (A) and $B220^+CD43^+$ precursor B-cells (B) in the bone marrow (BM) of WT mice (WT, n = 14) and C/EBPβ-KO mice (KO, n = 13), as determined by flow cytometric analysis. (C, D) Detailed flow cytometric analysis of subsets of B-cells in the BM of WT and C/EBPβ-KO mice. (C) Representative counter-plots. Numbers indicate the percentage of cells in boxes. (D) Percentages of pre-pro-B-cells (Fraction A), pro-B-cells (Fraction B/C), and pre-BI cells (Fraction C'). *, $P < 0.05$; **, $P < 0.01$.

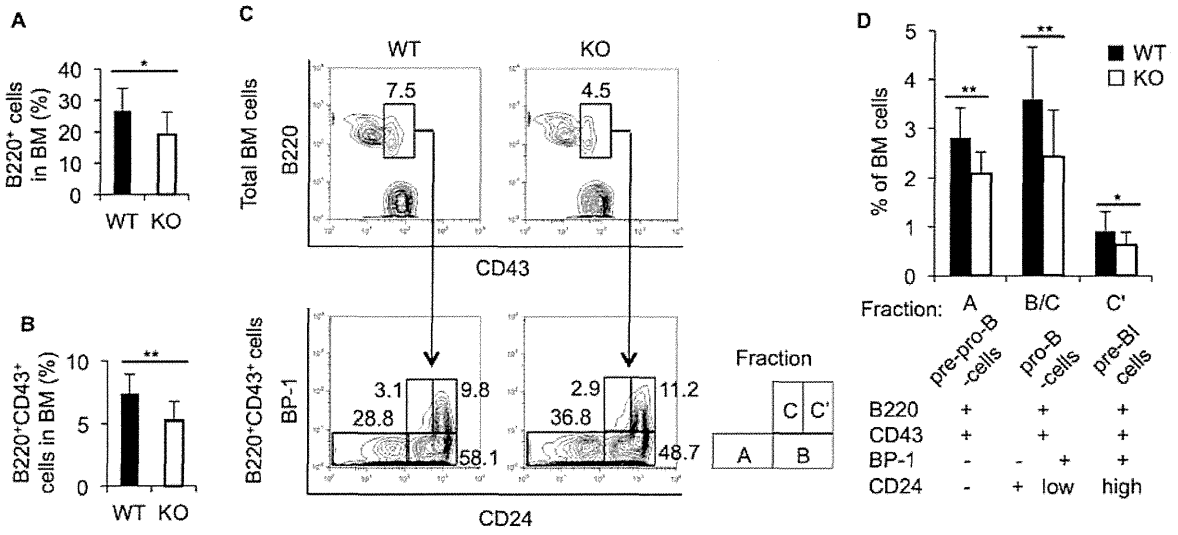

Figure 2. C/EBPβ-deficient bone marrow cells generate an equivalent level of B-cells as WT bone marrow cells when transplanted into WT mice. (A□C) BM transplantation experiments. (A) Schema of the BM transplantation experiments. WT mice, which provide a normal BM microenvironment, received BM hematopoietic cells (1×10^6 cells) from WT mice (WT→WT, n = 5) or C/EBPβ-KO mice (KO→WT, n = 3). The level of B-cells in the BM of recipient mice was analyzed 14 weeks after transplantation. (B) Percentage of $B220^+$ B-cells in the recipient BM of the WT→WT (closed bar) and the KO→WT (open bar) groups, as determined by flow cytometric analysis. (C) Detailed flow cytometric analysis of subsets of B-cells. Percentages of pre-pro-B-cells (Fraction A), pre-B-cells (Fraction B/C), and pre-BI cells (Fraction C') in the recipient BM of the WT→WT and KO→WT groups. (D□F) Competitive BM transplantation experiments. (D) Schema of the competitive BM transplantation experiments. GFP^- WT mice, which provide a normal bone marrow microenvironment, received BM cells from GFP^- WT mice (1×10^6 cells) and either GFP^+ WT mice (1×10^6 cells) (Transplantation-A, n = 5) or GFP^+ C/EBPβ-KO mice (1×10^6 cells) (Transplantation-B, n = 5). BM cells were analyzed 20 weeks after transplantation. (E) Percentage of GFP^+ cells engrafted in the recipient BM and spleen (SP), as determined by flow cytometric analysis. (F) Percentage of $B220^+$ cells engrafted in the recipient bone marrow (BM), as determined by flow cytometric analysis.

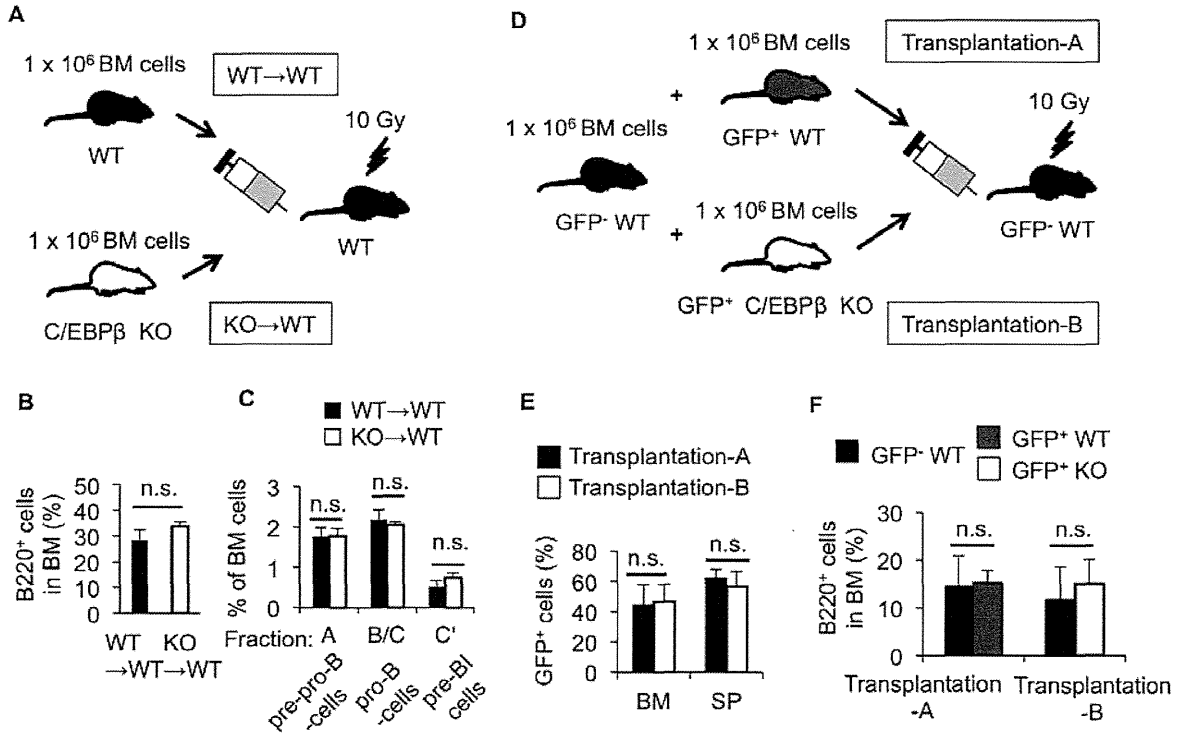

Figure 3. Differentiation of HSCs into precursor B-cells is impaired when co-cultured with C/EBPβ-deficient BMMSCs, in which CXCL12/SDF-1 production is reduced. KSL HSCs derived from WT (Ly5.1) mice (WT (Ly5.1)-KSL cells) were co-cultured with WT (Ly5.2) or C/EBPβ-deficient (KO) (Ly5.2) BMMSCs *in vitro* in the presence of SCF, Flt3-L and IL-7 with (SDF-1 +) or without (SDF-1 -) addition of CXCL12/SDF-1. Three experiments were performed in each condition. B-cell lymphopoiesis was analyzed after 10 days of co-culture. (A) Schema of co-culture experiments. (B) The number of hematopoietic cells generated from WT (Ly5.1)-KSL cells when co-cultured with WT (Ly5.2) or C/EBPβ-deficient (KO) (Ly5.2) BMMSCs, or cultured alone (BMMSCs (-)). (C, D) Flow cytometric analysis showing levels of $B220^+$ B-cells generated from WT (Ly5.1)-KSL cells when co-cultured with WT (Ly5.2) or C/EBPβ-deficient (KO) (Ly5.2) BMMSCs. (C) Representative counter plots. (E, F) Detailed flow cytometric analysis of the precursor B-cell population. Representative counter plots (E) and the percentages of B-cell subsets in $B220^+CD43^+$ precursor B-cells (F). (G) Quantitative real-time PCR analysis examining CXCL12/SDF-1 mRNA expression in BMMSCs. WT: WT BMMSCs (n = 6), KO: C/EBPβ-deficient BMMSCs (n = 6). **(H)** The protein concentration of CXCL12/SDF-1 was measured in the culture supernatant of WT BMMSCs (WT, n = 5) and C/EBPβ-deficient BMMSCs (KO, n = 5) by ELISA. **(I)** The number of $B220^+$ B-cells generated from WT-KSL cells strongly correlated with the concentration of CXCL12/SDF-1 in the culture supernatant. Numbers in each box indicate the percentage of cells (C, E). *, $P < 0.05$; **, $P < 0.01$.

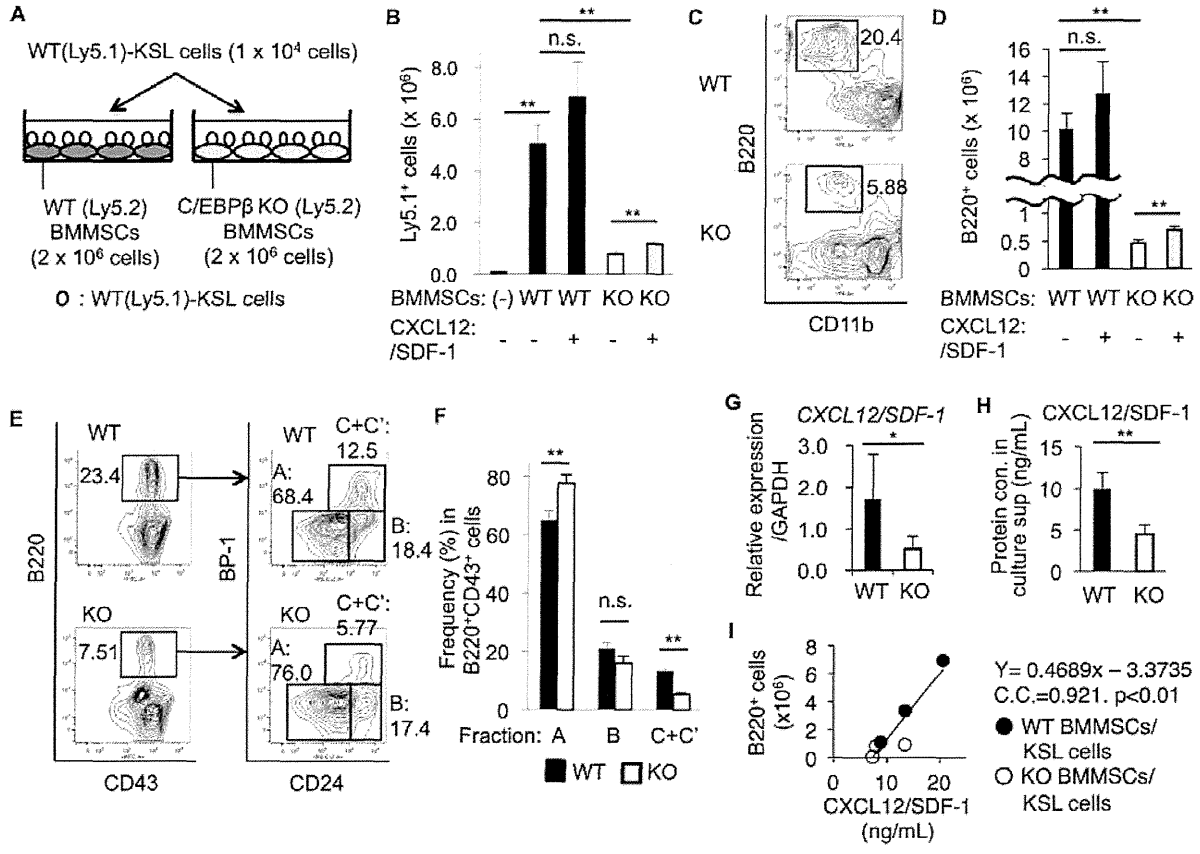

Figure 4. C/EBPβ-deficient BMMSCs have an impaired osteogenic differentiation capability. (A, B) Alizarin Red S staining of WT and C/EBPβ-deficient (KO) BMMSCs cultured in osteogenesis-inducing conditions *in vitro*. (A) Representative images. Yellow arrows indicate calcium deposits. Original magnification, 100×. Bars, 50 μm. (B) Calcium deposits were measured in ten different fields at 100× magnification. (C) Immunoblot analysis of Runx2 and ALP expression in WT and C/EBPβ-deficient (KO) BMMSCs cultured in osteogenesis-inducing conditions *in vitro*. Expression levels were measured using densitometry and normalized against the expression level of β-actin. (D) Quantitative real-time PCR analysis examining the expression of ALP mRNA in BMMSCs cultured in osteogenesis-inducing conditions *in vitro*. WT: WT BMMSCs (n = 3), KO: C/EBPβ-deficient BMMSCs (n = 5). (E, F) *In vivo* bone-forming capability of BMMSCs. WT or C/EBPβ-deficient BMMSCs mixed with HA/TCP were subcutaneously implanted into SCID mice. (E) Representative macroscopic appearance of BMMSC implants (left panels). Yellow arrows indicate osseous nodules. Representative microscopic images of sections of BMMSC implants stained with HE (right panels). Original magnification, 40×. Bars, 50 μm. Yellow asterisks indicate bone-forming areas. (F) Bone formation in WT BMMSC implants (WT, n = 6) and C/EBPβ-deficient BMMSC implants (KO, n = 4), as assessed by HE staining. Bone-forming areas at 40× magnification were quantified using Image J software. **, $P < 0.01$.

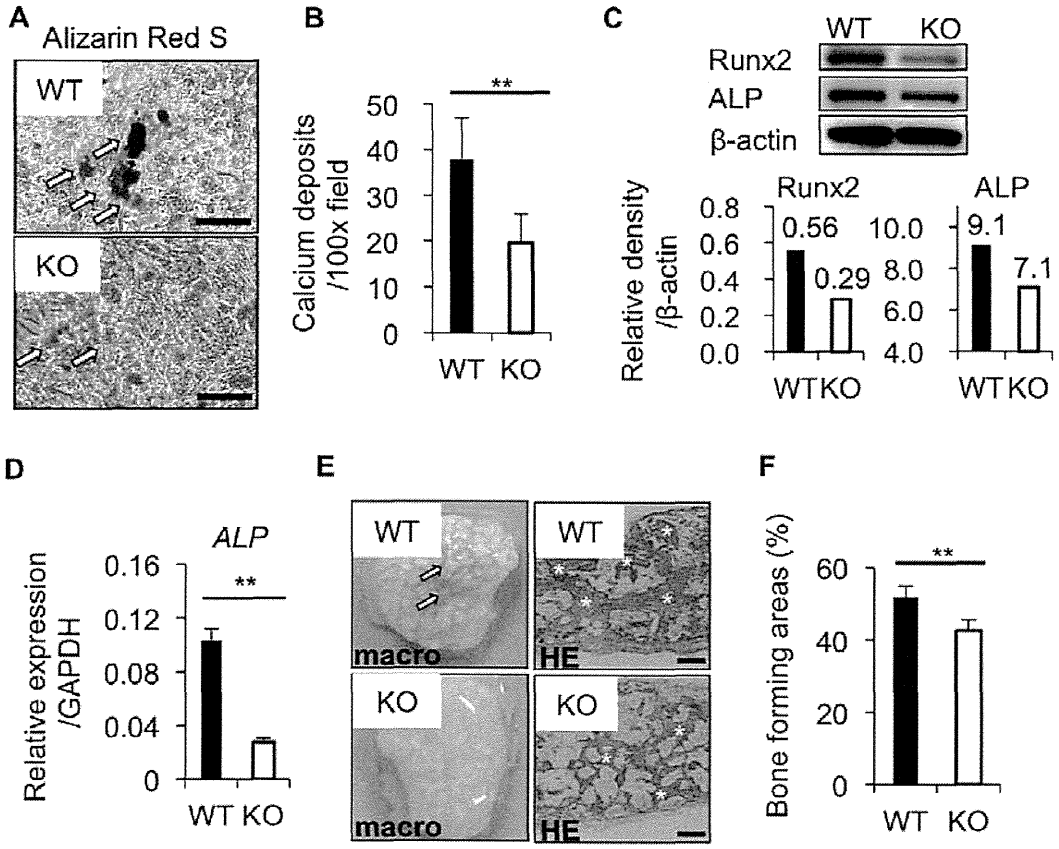

Figure 5. C/EBPβ-deficient BMMSCs have an impaired adipogenic differentiation capability. (A-C) Culture of WT and C/EBPβ-deficient (KO) BMMSCs in adipogenesis-inducing conditions *in vitro*. (A) Representative phase contrast images. Yellow arrows indicate lipid deposition. Original magnification, 100×. Bars, 50 μm. (B, C) Oil Red O staining of WT and C/EBPβ-deficient (KO) BMMSCs cultured in adipogenesis-inducing conditions. (B) Representative images. Yellow arrows indicate lipid deposits. Original magnification, 100×. Bars, 50 μm. (C) The number of Oil Red O^+ cells was measured in ten different fields at 100× magnification. (D) Immunoblot analysis examining the expression of PPARγ, Lpl, and FABP4 in WT and C/EBPβ-deficient (KO) BMMSCs cultured in adipogenesis-inducing conditions *in vitro*. Expression levels were determined using densitometry and normalized against the expression level of β-actin. (E) Quantitative real-time PCR analysis examining the expression of PPARγ, Lpl, and Fabp4 mRNA in BMMSCs cultured in adipogenesis-inducing conditions. WT: WT BMMSCs (n = 5), KO: C/EBPβ-deficient BMMSCs (n = 5). *, $P < 0.05$; **, $P < 0.01$.

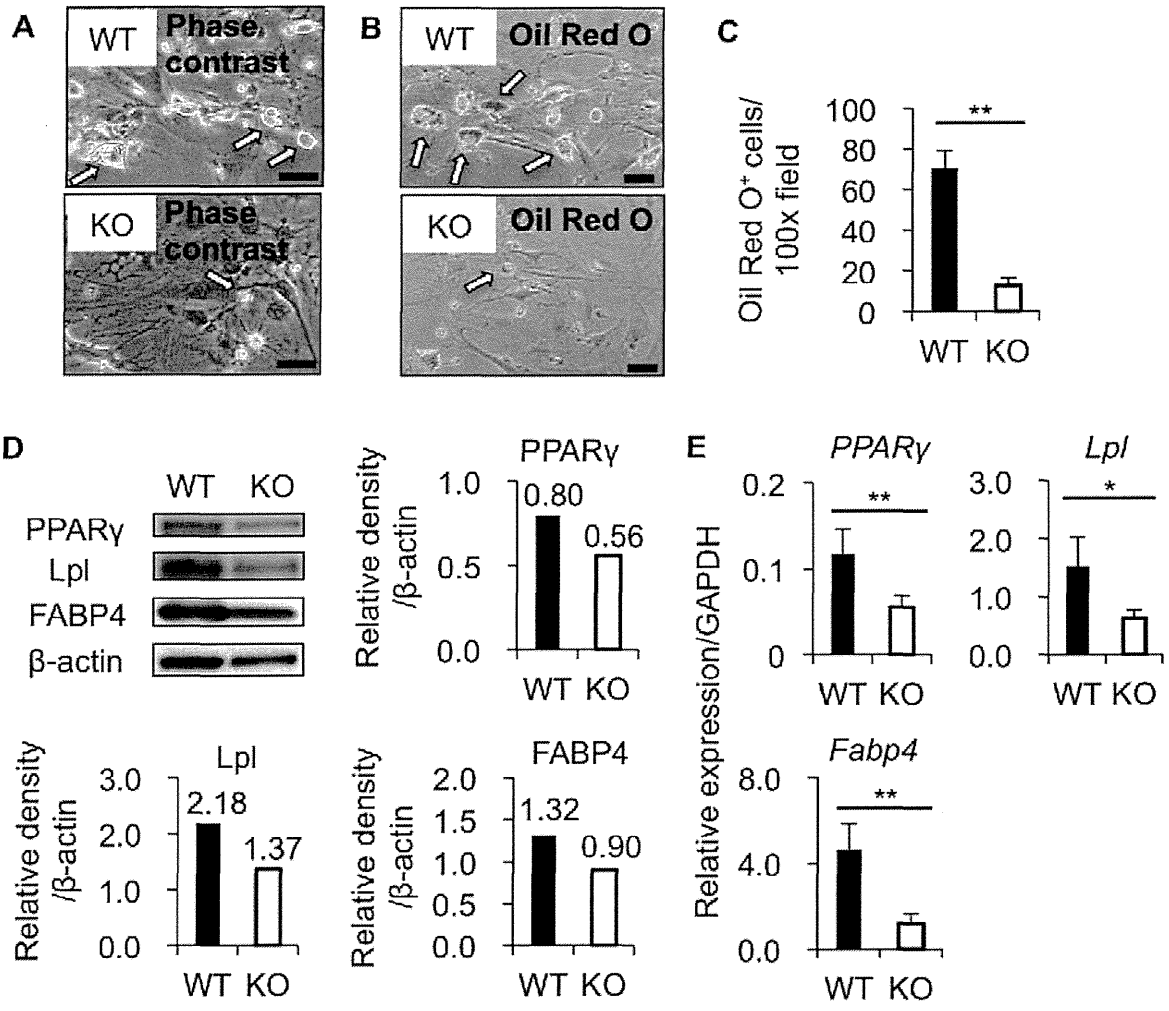

Figure 6. Survival of leukemic precursor B-cells is suppressed when co-cultured with C/EBPβ-deficient BMMSCs. (A) BaF3/Bcr-Abl cells were co-cultured with WT or C/EBPβ-deficient (KO) BMMSCs. (B) Number of BaF3/Bcr-Abl cells when co-cultured with WT (WT, n = 5) or C/EBPβ-deficient (KO) (n = 5) BMMSCs. (C, D) Cell cycle analyses of BaF3/Bcr-Abl cells after co-culture with WT (n = 5) or C/EBPβ-deficient (KO) (n = 5) BMMSCs for 2 days. (C) Representative histograms. (D) The frequencies of BaF3/Bcr-Abl cells at G0/G1, S and G2M phases. Data are mean values ± SD. (F, G) Frequency of apoptotic BaF3/Bcr-Abl cells after co-culture with WT (n = 5) or C/EBPβ-deficient (KO) (n = 5) BMMSCs for 3days. (E) Representative counter plots. Numbers in each box indicate the percentage of cells. (F) Frequencies of Annexin V^-PI^-, Annexin V^+PI^-, and Annexin V^+PI^+ cells. Data are mean absorbance values ± SD. (G) The number of BaF3/Bcr-Abl cells stimulated with exogenous CXCL12/SDF-1 was examined by determing BrdU incorporation using a colorimetric immunoassay (n = 6). Data are mean absorbance values ± SD. *, $P < 0.05$; **, $P < 0.01$.

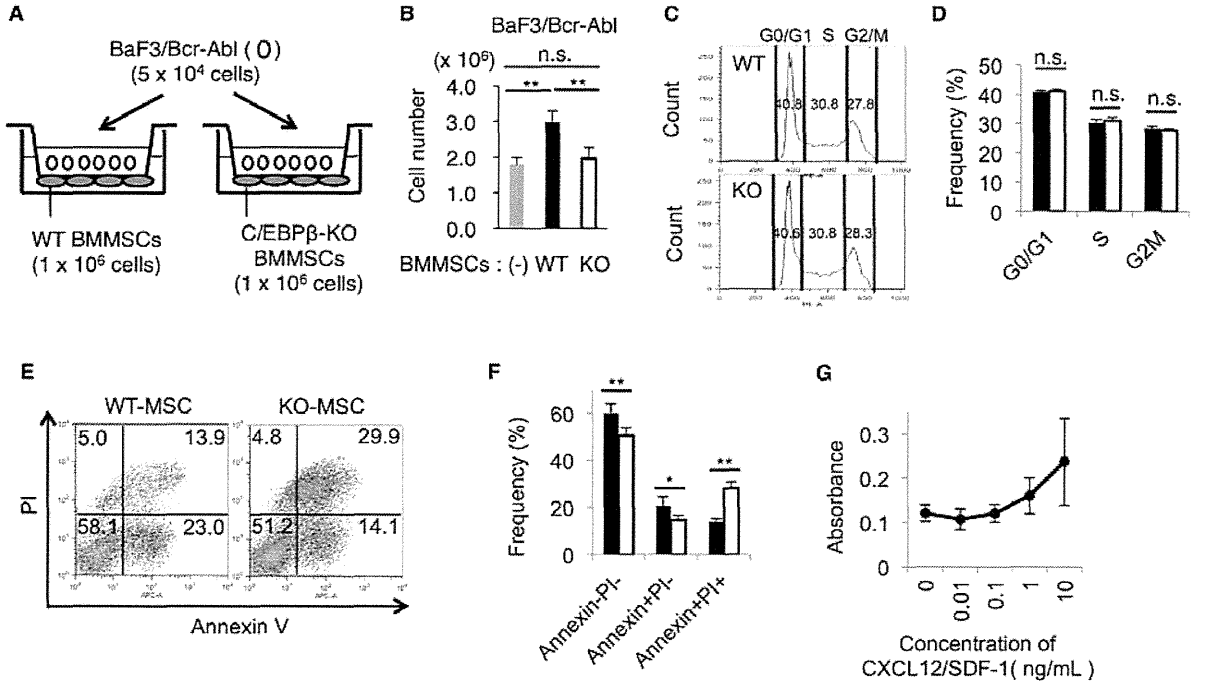

Biochemical and Biophysical Research Communications xxx (2013) xxx–xxx

Contents lists available at ScienceDirect

Biochemical and Biophysical Research Communications

journal homepage: www.elsevier.com/locate/ybbrc

Uric acid induces NADPH oxidase-independent neutrophil extracellular trap formation

Yasuyuki Arai [a,1], Yoko Nishinaka [b,c,1], Toshiyuki Arai [a,d], Makiko Morita [b], Kiyomi Mizugishi [a], Souichi Adachi [b], Akifumi Takaori-Kondo [a], Tomohiro Watanabe [e], Kouhei Yamashita [a,*]

[a] Department of Hematology and Oncology, Graduate School of Medicine, Kyoto University, Kyoto 606-8507, Japan
[b] Human Health Science, Graduate School of Medicine, Kyoto University, Kyoto 606-8507, Japan
[c] Department of Clinical Application, Center for iPS Cell Research and Application, Kyoto University, Kyoto 606-8507, Japan
[d] Department of Anesthesia, Kyoto City Hospital, Kyoto 604-8845, Japan
[e] Center for Innovation in Immunoregulative Technology and Therapeutics, Graduate School of Medicine, Kyoto University, Kyoto 606-8507, Japan

ARTICLE INFO

Article history:
Received 15 November 2013
Available online xxxx

Keywords:
Uric acid
Neutrophil extracellular trap formation
NADPH oxidase
Chronic granulomatous disease
NF-κB
Reactive oxygen species

ABSTRACT

Neutrophil extracellular traps (NETs) are composed of extracellular DNA fibers with antimicrobial peptides that capture and kill microbes. NETs play a critical role in innate host defense and in autoimmune and inflammatory diseases. While the mechanism of NET formation remains unclear, reactive oxygen species (ROS) produced via activation of NADPH oxidase (Nox) are known to be an important requirement. In this study, we investigated the effect of uric acid (UA) on NET formation. UA, a well-known ROS scavenger, was found to suppress Nox-dependent ROS release in a dose-dependent manner. Low concentrations of UA significantly inhibited Nox-dependent NET formation. However, high concentrations of UA unexpectedly induced, rather than inhibited, NET formation. NETs were directly induced by UA alone in a Nox-independent manner, as revealed by experiments using control neutrophils treated with ROS inhibitors or neutrophils of patients with chronic granulomatous disease who have a congenital defect in ROS production. Furthermore, we found that UA-induced NET formation was partially mediated by NF-κB activation. Our study is the first to demonstrate the novel function of UA in NET formation and may provide insight into the management of patients with hyperuricemia.

1. Introduction

Neutrophils, the first line of defense against the microbes, play a critical role in innate immunity [1]. In infected sites, they phagocytose microbes, degranulate enzymes, and produce reactive oxygen species (ROS) such as superoxide and hydrogen peroxide generated by the NADPH oxidase (Nox) complex. Recently, a novel killing mechanism known as neutrophil extracellular traps (NETs) has been reported. NETs capture microbes with their extracellular structures consisting of DNA fibers and antimicrobial granule proteins [2,3]. Many physiological stimuli are known to induce NETs. Notably, NET formation is generally ROS-dependent. Patients with chronic granulomatous disease (CGD), who are defective in Nox activity, fail to generate ROS and to make NETs [4]. In a recent study, we demonstrated that singlet oxygen ($^1O_2$), one species of ROS, is required for Nox-dependent NET formation on stimulation with phorbol myristate acetate (PMA) [5]. Interestingly, neutrophils of CGD patients treated with $^1O_2$ *in vitro* produced NETs, revealing that the pathway could be rescued downstream of Nox [5].

Uric acid (UA), a product of purine metabolism, is a scavenger of $^1O_2$ that regulates oxidative stress in humans [6]. Since $^1O_2$ is produced by Nox [7], UA is expected to suppress Nox-dependent NET formation. However, a recent study showed that peripheral and synovial fluid neutrophils derived from patients with acute gout, whose UA levels in serum were mostly high, formed NETs [8]. Acute gout is an inflammatory arthritis that is triggered by the deposition of monosodium urate (MSU) crystals, uric acid precipitates in sodium, into the joint space. The inflammatory cascade results in the secretion of inflammatory cytokines, especially interleukin (IL)-1ß and neutrophil recruitment into the joint [9]. Thus, it is still a matter of debate what effect UA directly exerts on NET formation.

In the present study, we first examined the effect of UA on Nox-dependent NET formation by control neutrophils stimulated with PMA. Thereafter, we investigated how UA directly affected NET for-

Abbreviations: CGD, chronic granulomatous disease; DHR, dihydrorhodamine 123; DPI, diphenyleneiodonium; HBSS, Hanks' balanced salt solution; MSU, monosodium urate; MVP, trans-1-(2′-methoxyvinyl)pyrene; Nox, NADPH oxidase; NET, neutrophil extracellular trap; PBN, α-phenyl-*N*-tert-butyl nitrone; PMA, phorbol myristate acetate; ROS, reactive oxygen species; $^1O_2$, singlet oxygen; UA, uric acid.

* Corresponding author. Fax: +81 75 751 4963.
E-mail address: kouhei@kuhp.kyoto-u.ac.jp (K. Yamashita).

[1] These authors contributed equally to this work.

0006-291X/$ - see front matter © 2013 Elsevier Inc. All rights reserved.
http://dx.doi.org/10.1016/j.bbrc.2013.12.007

mation by using control neutrophils treated with ROS inhibitors or CGD neutrophils. Finally, we demonstrate that UA may induce NET formation in a manner distinct from that of PMA.

2. Materials and methods

2.1. Reagents

Hanks' balanced salt solution (HBSS) was purchased from Invitrogen (Carlsbad, CA, USA); trans-1-(2′-methoxyvinyl)pyrene (MVP), Sytox green and orange (for double-strand DNA staining), and dihydrorhodamine 123 (DHR) were ordered from Molecular Probes (Eugene, OR, USA). α-Phenyl-*N*-tert-butyl nitrone (PBN) was acquired from Radical Research Ltd. (Hino, Tokyo, Japan) and was dissolved in phosphate-buffered saline (PBS) at a final concentration of 100 mM (pH 7.4). Anti-myeloperoxidase (MPO) antibody and matched secondary antibody (anti-rabbit IgG-Alexa Fluor 488) were obtained from Abcam (Eugene, OR, USA) and Life Technologies (Carlsbad, CA, USA), respectively. Other chemicals, including UA, PMA, diphenyleneiodonium (DPI), and apocynin, were purchased from Sigma Aldrich Inc. (St. Louis, MO, USA). (*E*)3-[(4-Methylphenyl)sulfonyl]-2-propenenitrile (BAY 11-7082) was obtained from Merck (Darmstadt, Germany).

2.2. Human CGD patients

We studied two CGD patients, a 29-year-old man with gp91-phox deficiency with a G-to-A point mutation at nucleotide 252 in exon 3, and a 24-year-old man with gp91-phox deficiency with a G-to-A point mutation at nucleotide 389 in exon 10.

2.3. Isolation of human neutrophils

Human neutrophils were isolated from peripheral blood by sedimentation through two-step Percoll (GE Healthcare, Tokyo, Japan) gradients. The experiments were conducted with the understanding and the consent of each participant. The ethical committee of Kyoto University approved the experiments.

2.4. Chemiluminescence assay

Neutrophils (2×10^6 cells) were mounted on a luminescence reader (Aloka BLR-310; Aloka, Tokyo, Japan) in the presence of 40 μM MVP, a $^1O_2$-specific probe [10]. After that, neutrophils were stimulated with 100 ng/ml PMA in the presence of 0–5 mg/dl UA, or 8 mg/dl UA alone, and MVP luminescence was monitored every 30 s for 30 min.

2.5. Flow cytometric DHR assay

Neutrophils (1×10^6 cells) treated with 2 μM DHR were stimulated with 100 ng/ml PMA or 8 mg/dl UA for 30 min at 37 °C and analyzed by flow cytometry using a FACSCanto II (Becton Dickinson, Durham, NC, USA).

2.6. Immunofluorescence stainings of NET-forming neutrophils

Purified neutrophils (1×10^5 cells) were incubated with 100 ng/ml PMA or 8 mg/dl UA in HBSS without serum for 3 h on culture slides (BD Biosciences, San Jose, CA, USA). After fixation with 2% paraformaldehyde (Nacalai Tesque, Kyoto, Japan) for 15 min and

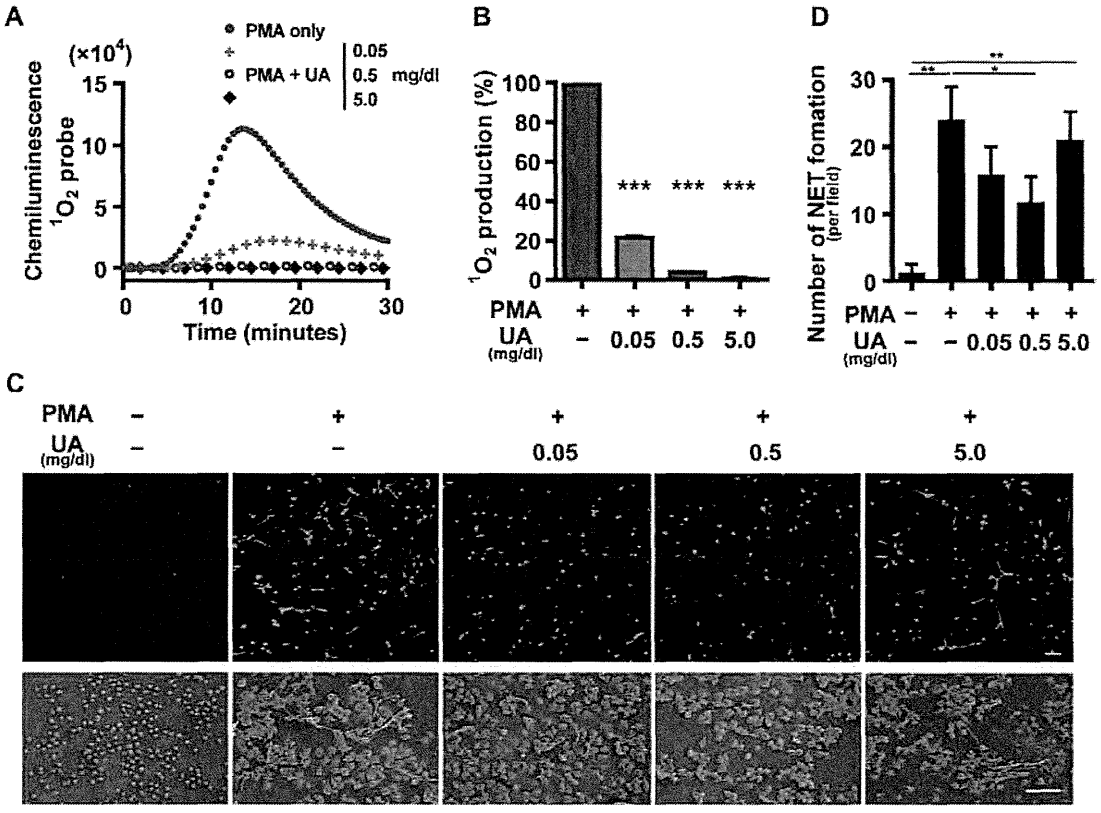

Fig. 1. The effect of UA on PMA-induced ROS production and NET formation. Neutrophils were isolated from the peripheral blood of healthy volunteers. (A) The effect of UA (0–5 mg/dl) on $^1O_2$ production by PMA-stimulated neutrophils. The $^1O_2$ production by neutrophils was examined by chemiluminescence using a $^1O_2$-specific probe, MVP. (B) Quantitative analysis of $^1O_2$ production by neutrophils. The $^1O_2$ production is shown relative to that by PMA-stimulated neutrophils in the absence of UA. The data represent the mean ± SE ($n = 3$, $^{***}P < 0.001$, unpaired *t*-test). (C) The effect of UA on PMA-induced NET formation. Neutrophils stimulated with PMA were incubated with 0–5 mg/dl UA. NET formation was visualized by laser-scanning fluorescence confocal microscopy (upper panels) and SEM (lower panels). Scale bars represent 100 μm (upper panels) and 30 μm (lower panels). (D) Quantitative analysis of NET formation. The data represent the mean ± SE ($n = 4$, $^{*}P < 0.05$, $^{**}P < 0.01$, unpaired *t*-test).

Please cite this article in press as: Y. Arai et al., Uric acid induces NADPH oxidase-independent neutrophil extracellular trap formation, Biochem. Biophys. Res. Commun. (2013), http://dx.doi.org/10.1016/j.bbrc.2013.12.007

permeabilization with 100% methanol (Nacalai Tesque) for 10 min at -20 °C, the cells were stained with rabbit anti-MPO antibodies overnight at 4 °C, followed by Alexa Fluor 488-conjugated goat anti-rabbit IgG and Sytox orange. The cells were attached to the slides by centrifugation, coverslipped with mounting medium (ProLong Gold Antifade Reagent, Life Technologies), and analyzed by confocal microscopy.

2.7. NET formation by neutrophils

Neutrophils (4×10^6 cells) from healthy volunteers were suspended in HBSS without serum and stimulated with 100 ng/ml PMA in the presence of 0–5 mg/dl UA for 3 h at 37 °C under 5% CO_2 in glass base dish (Asahi Glass, Tokyo, Japan). In other experiments, neutrophils from healthy volunteers or CGD patients were stimulated with 1–8 mg/dl UA alone. After incubation, cells were stained with 500 nM Sytox Green, and NET formation was visualized with a laser-scanning fluorescence confocal microscope (Nikon Digital Eclipse C1, Tokyo, Japan). Quantitative analysis was performed by counting the number of NET-forming cells per field (average data of 5 randomly selected fields). NET formation was also visualized with a scanning electron microscope (SEM, S-4700, Hitachi, Tokyo, Japan).

2.8. Treatments of neutrophils with inhibitors

Neutrophils (4×10^6 cells) from healthy volunteers were pre-incubated at 37 °C for 30 min with Nox inhibitors, DPI (10 μM) and apocynin (10 μM), a $^1O_2$ inhibitor, PBN (4 mM) [11], or an NF-κB inhibitor, Bay 11-7082 (10 μM), and then stimulated with 100 ng/ml PMA or 8 mg/dl UA for 3 h. NET formation was visualized and analyzed as described above.

2.9. Immunoblotting

Neutrophils (4×10^6 cells) from healthy volunteers were incubated at 37 °C for 30 min with 100 ng/ml PMA or 8 mg/dl UA. Lysates were prepared using RIPA lysis buffer (Wako Pure Chemical Industries, Osaka, Japan). Cell debris was separated by centrifugation and equal amounts of proteins in the supernatant were separated by electrophoresis (4–12% SDS–polyacrylamide gels, Life Technologies). Proteins were then electrotransferred onto nitrocel-

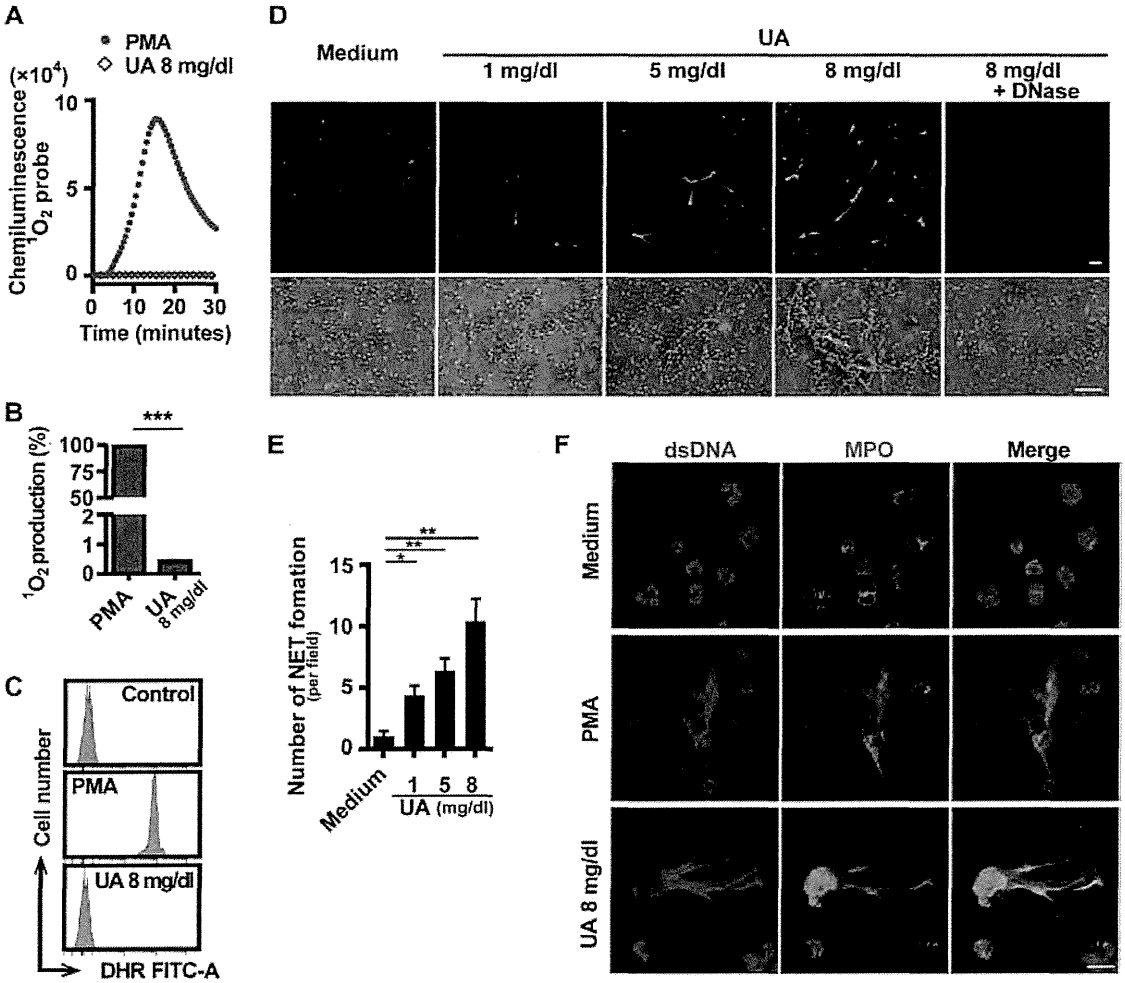

Fig. 2. The effect of UA alone on ROS production and NET formation. (A and B) Effect of UA on $^1O_2$ production. Neutrophils were stimulated with PMA (100 ng/ml) or UA (8 mg/dl). $^1O_2$ production was examined by chemiluminescence using a $^1O_2$-specific probe, MVP. (A) Representative data. UA-stimulated neutrophils hardly produced any $^1O_2$. (B) Quantitative analysis of $^1O_2$ production shown relative to that by PMA-stimulated neutrophils. Data represent mean ± SE ($n = 3$, $^{***}P < 0.001$, unpaired t-test). (C) ROS production by DHR assay. The logarithmic fluorescence intensity is shown on the x-axis and the cell count on the y-axis. (D–F) Direct effect of UA on NET formation. (D) Representative micrographs of neutrophils incubated with 1–8 mg/dl of UA. NET formation was visualized by laser-scanning fluorescence confocal microscopy (upper panels) and SEM (lower panels). Scale bars represent 100 μm (upper panels) and 30 μm (lower panels). (E) Quantitative analysis of NET formation. Data represent the mean ± SE ($n = 5$, $^{*}P < 0.05$, $^{**}P < 0.01$, unpaired t-test). (F) Colocalization of extracellular dsDNA and MPO in UA-stimulated neutrophils. UA- or PMA-stimulated neutrophils were immunostained with anti-MPO antibody (green). The dsDNAs were counterstained with Sytox-orange (red). Scale bars represent 10 μm. (For interpretation of the references to color in this figure legend, the reader is referred to the web version of this article.)

Please cite this article in press as: Y. Arai et al., Uric acid induces NADPH oxidase-independent neutrophil extracellular trap formation, Biochem. Biophys. Res. Commun. (2013), http://dx.doi.org/10.1016/j.bbrc.2013.12.007

lulose membranes. After blocking, membranes were incubated overnight at 4 °C with a rabbit polyclonal anti-phospho-NF-κB p65 or anti-NF-κB p65 antibody (Santa Cruz Biotechnology, Dallas, TX, USA) followed by a goat anti-rabbit HRP antibody. Protein bands were visualized by enhanced chemiluminescence, and results were analyzed with ImageJ software.

2.10. Statistical analysis

Data were expressed as mean ± standard error (SE). Values of $P < 0.05$ determined by the unpaired Student t-test were considered significant.

3. Results and discussion

We examined the effect of UA on $^1O_2$ production and NET formation by PMA-stimulated neutrophils. First, neutrophils from healthy volunteers were stimulated with PMA with or without UA, and the $^1O_2$ production was detected by chemiluminescence. As expected, increasing concentrations of UA (0.05–5 mg/dl) suppressed $^1O_2$ production by PMA-stimulated neutrophils in a dose-dependent manner, suggesting that UA is a $^1O_2$ scavenger (Fig. 1A and B). Treatments of less than 0.5 mg/dl of UA suppressed PMA-induced NET formation in confocal microscopy (Fig. 1C, upper panels, and Fig. 1D) and SEM (Fig. 1C, lower panels). Surprisingly, treatment of PMA-stimulated neutrophils with 5 mg/dl of UA failed to suppress NET formation, suggesting that a high concentration of UA may have a novel function in NET formation (Fig. 1C and D). These results were substantiated by the quantitative analysis of representative micrographs (Fig. 1D).

Next, we investigated the direct effect of UA on $^1O_2$ production and NET formation. UA treatment alone did not produce any detectable levels of $^1O_2$ (Fig. 2A and B). We used the fluorescent dye DHR in a flow cytometric assay to detect ROS. UA-stimulated neutrophils from healthy volunteers did not exhibit any increase in DHR fluorescence, in contrast to a significant increase in PMA-stimulated neutrophils (Fig. 2C). Unexpectedly, UA alone

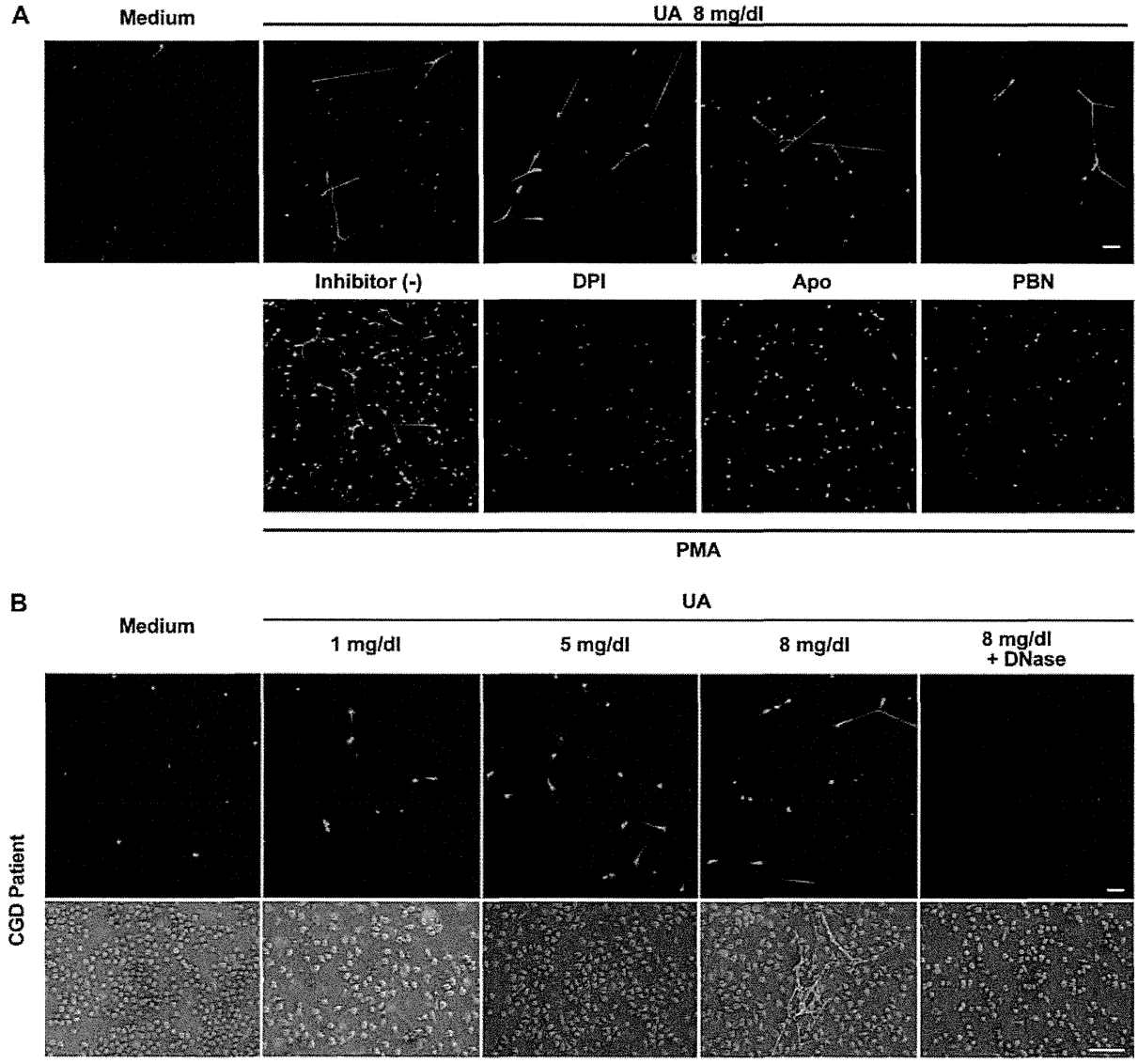

Fig. 3. UA-induced NET formation is independent of ROS. (A) The effect of ROS inhibitors on UA- (upper panels) or PMA- (lower panels) induced NET formation. Neutrophils from healthy volunteers were incubated with 8 mg/dl UA or 100 ng/ml PMA in the presence or absence of Nox inhibitors, DPI and apocynin (Apo), or a $^1O_2$ inhibitor, PBN. NET formation was visualized by laser-scanning fluorescence confocal microscopy. Scale bars represent 100 μm. (B) The effect of UA on NET formation. Neutrophils from CGD patients were incubated with 1–8 mg/dl of UA. Representative micrographs are shown. NET formation was visualized by laser-scanning fluorescence confocal microscopy (upper panels) and SEM (lower panels). Scale bars represent 100 μm (upper panels) and 30 μm (lower panels).

Please cite this article in press as: Y. Arai et al., Uric acid induces NADPH oxidase-independent neutrophil extracellular trap formation, Biochem. Biophys. Res. Commun. (2013), http://dx.doi.org/10.1016/j.bbrc.2013.12.007

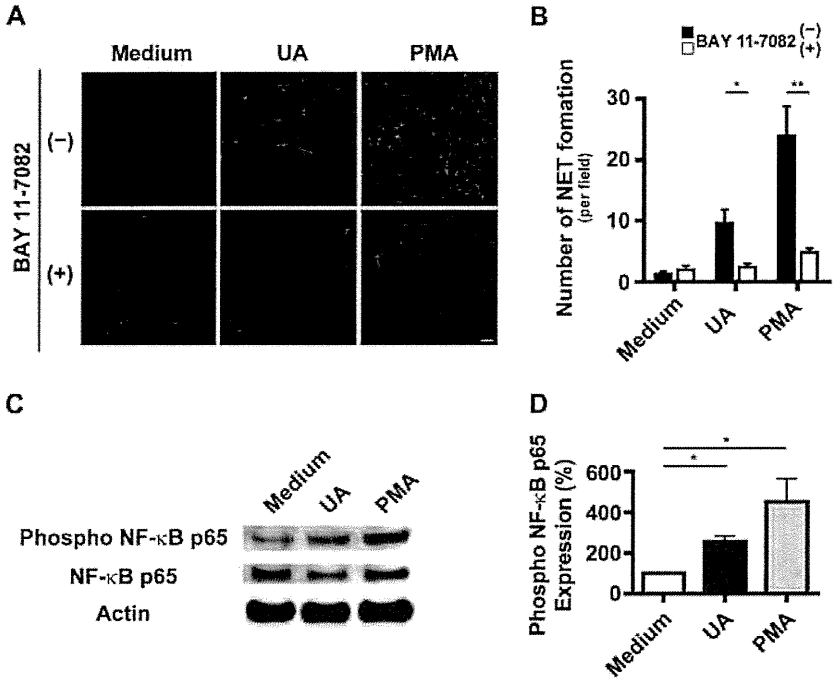

Fig. 4. UA induces NET formation through NF-κB activation. (A and B) The effect of an NF-κB inhibitor on UA-induced NET formation. Neutrophils from healthy volunteers were stimulated with 100 ng/ml PMA or 8 mg/dl UA in the presence or absence of an NF-κB inhibitor. (A) Representative micrographs. NET formation was visualized by laser-scanning fluorescence confocal microscopy. Scale bars represent 100 μm. (B) Quantitative analysis of NET formation. The data represent the mean ± SE ($n = 5$, $^{*}P < 0.05$, $^{**}P < 0.01$, unpaired t-test). (C) Immunoblot analysis of PMA- or UA-stimulated neutrophils. Cell lysates were subjected to immunoblotting using an anti-phospho-NF-κB p65 or anti-NF-κB p65 antibody. Membranes were reprobed with an anti-actin antibody. (D) Quantification of proteins on immunoblots. The expression levels are shown relative to that in neutrophils without stimuli. The data represent the mean ± SE ($n = 5$, $^{*}P < 0.05$, unpaired t-test).

significantly induced NET formation in healthy neutrophils, irrespective of the absence of ROS (Fig. 2D and E). NET formation was abrogated by DNase treatment, which degrades DNA fibers of NETs (Fig. 2D). NET formation by UA was further verified by immunostaining, in which extracellular dsDNA colocalized with a granule protein MPO, an important structural component of NETs (Fig. 2F). These results suggest that NET formation by UA may not be mediated by ROS.

This hypothesis was substantiated by the use of Nox inhibitors, DPI and apocynin, or a $^{1}O_2$ scavenger, PBN. None of the ROS inhibitors suppressed UA-induced NET formation, while PMA-induced NETs were strongly inhibited (Fig. 3A). We next examined NET formation in neutrophils from CGD patients, who have a defect in ROS formation. Regardless of the absence of ROS, CGD neutrophils treated with UA produced NETs, which were suppressed by DNase treatment (Fig. 3B). Taken together, these results suggest that UA may induce NET formation in a Nox-independent manner.

Recently, Lopponi et al. implicated NF-κB activation in NET formation induced by PMA stimulus or stress signals, such as acidic or hyperthermic conditions [12]. Therefore, we investigated whether NF-κB blockade affected NET formation by UA-stimulated neutrophils. The treatment of healthy neutrophils with the NF-κB inhibitor BAY 11-7082 resulted in a marked suppression of UA-induced NET formation (Fig. 4A and B). In addition, immunoblot analysis revealed that phosphorylation of the p65 subunit of NF-κB was significantly enhanced in neutrophils stimulated with UA (Fig. 4C and D). Taken together, these results suggest that the NF-κB cascade is important in UA-mediated NET formation, and could be a key regulatory pathway of NET formation. Identification of signaling pathways upstream of NF-κB in UA-induced NET formation should be a future area of investigation.

In summary, this is the first report to demonstrate the novel function of UA in NET formation. Contrary to expectations, UA, a known $^{1}O_2$ scavenger, induced NETs in neutrophils in a Nox-independent manner and partially through activation of the NF-κB pathway. The mechanisms by which UA contributes to NET formation are not yet clear. It has been reported that the Raf-MEK-ERK pathway is involved in a NET formation cascade downstream of Nox activation in PMA-stimulated neutrophils [13]. Furthermore, MSU crystals induced NETs in a ROS-dependent manner as well as PMA [14]. In contrast, NET formation by UA was independent of ROS. In addition, neither the activation of ERK, nor the suppression of NETs by an ERK inhibitor, was observed in UA-stimulated neutrophils in our study (unpublished observation). This suggests that UA induces NETs in a different fashion from that of PMA and MSU crystals. An example of ROS-independent NET formation was reported in a recent study, where the calcium ionophore ionomycin did not require Nox activation to induce NETs [15]. Moreover, *Staphylococcus aureus* and *Candida albicans* have been reported to induce NETs independently of Nox [16,17]. Thus, it is possible that there are several mechanisms of NET formation. The importance of a ROS-independent pathway in NET formation in physiological settings awaits further investigation.

NETs are similar to a double-edged sword; they can either fight disease or cause disease, depending on the situation [18]. Excessive NET formation is associated with the pathogenesis of inflammatory and autoimmune diseases, including preeclampsia [19], cystic fibrosis [20], and systemic lupus erythematosus [21]. Moreover, NETs are relevant to vascular injury, in which extracellular histones released from neutrophils during NET formation injure the endothelium [22], and the injured endothelium, in turn, induces NETs, establishing a vicious cycle leading to severe damage [23]. Clinically, the association of hyperuricemia and gout with other medical conditions such as hypertension, chronic kidney disease, and cardiovascular disease has been recognized [24]. Recent animal and epidemiologic studies support the idea that uric acid elevation in the serum is an independent risk factor for the development of these serious medical problems, by damaging

Please cite this article in press as: Y. Arai et al., Uric acid induces NADPH oxidase-independent neutrophil extracellular trap formation, Biochem. Biophys. Res. Commun. (2013), http://dx.doi.org/10.1016/j.bbrc.2013.12.007

endothelial cells, although it is still a matter of debate [25]. In light of these findings, we speculate that uric acid elevation may induce NET formation and subsequent vascular endothelial dysfunction, ultimately leading to cardiovascular diseases. Therefore, NETs could be a missing link between uric acid elevation and cardiovascular diseases. Thus, we may need to reappraise the importance of uric acid in human health and disease, and reconsider the management of patients with asymptomatic hyperuricemia in order to decrease the risk of cardiovascular diseases.

Conflict of interest disclosure

The authors declare no conflict of interest.

Acknowledgments

We thank Keiko Furuta and Haruyasu Kohda (Division of Electron Microscopic Study, Center for Anatomical Studies, Graduate School of Medicine, Kyoto University) for excellent technical assistance. This research was supported by Grants-in-aid for scientific research from the Japan Society for the Promotion of Science (23591474) to K.Y.

References

[1] C. Nathan, Neutrophils and immunity: challenges and opportunities, Nat. Rev. Immunol. 6 (2006) 173–182.
[2] V. Brinkmann, U. Reichard, C. Goosmann, B. Fauler, Y. Uhlemann, D.S. Weiss, Y. Weinrauch, A. Zychlinsky, Neutrophil extracellular traps kill bacteria, Science 303 (2004) 1532–1535.
[3] V. Brinkmann, A. Zychlinsky, Beneficial suicide: why neutrophils die to make NETs, Nat. Rev. Microbiol. 5 (2007) 577–582.
[4] T.A. Fuchs, U. Abed, C. Goosmann, R. Hurwitz, I. Schulze, V. Wahn, Y. Weinrauch, V. Brinkmann, A. Zychlinsky, Novel cell death program leads to neutrophil extracellular traps, J. Cell Biol. 176 (2007) 231–241.
[5] Y. Nishinaka, T. Arai, S. Adachi, A. Takaori-Kondo, K. Yamashita, Singlet oxygen is essential for neutrophil extracellular trap formation, Biochem. Biophys. Res. Commun. 413 (2011) 75–79.
[6] B.N. Ames, R. Cathcart, E. Schwiers, P. Hochstein, Uric acid provides an antioxidant defense in humans against oxidant- and radical-caused aging and cancer: a hypothesis, Proc. Natl. Acad. Sci. U.S.A. 78 (1981) 6858–6862.
[7] S.J. Klebanoff, Myeloperoxidase: friend and foe, J. Leukocyte Biol. 77 (2005) 598–625.
[8] I. Mitroulis, K. Kambas, A. Chrysanthopoulou, P. Skendros, E. Apostolidou, I. Kourtzelis, G.I. Drosos, D.T. Boumpas, K. Ritis, Neutrophil extracellular trap formation is associated with IL-1beta and autophagy-related signaling in gout, PLoS One 6 (2011) e29318.
[9] E.B. Gonzalez, An update on the pathology and clinical management of gouty arthritis, Clin. Rheumatol. 31 (2012) 13–21.
[10] G.H. Posner, J.R. Lever, K. Miura, C. Lisek, H.H. Seliger, A. Thompson, A chemiluminescent probe specific for singlet oxygen, Biochem. Biophys. Res. Commun. 123 (1984) 869–873.
[11] A. Kawai, Y. Nishinaka, T. Arai, K. Hirota, H. Mori, N. Endo, T. Miyoshi, K. Yamashita, M. Sasada, Alpha-phenyl-*N*-tert-butyl nitrone has scavenging activity against singlet oxygen ((1)O(2)) and attenuates (1)O(2)-induced neuronal cell death, J. Pharmacol. Sci. 108 (2008) 545–549.
[12] M.J. Lapponi, A. Carestia, V.I. Landoni, L. Rivadeneyra, J. Etulain, S. Negrotto, R.G. Pozner, M. Schattner, Regulation of neutrophil extracellular trap formation by anti-inflammatory drugs, J. Pharmacol. Exp. Ther. 345 (2013) 430–437.
[13] A. Hakkim, T.A. Fuchs, N.E. Martinez, S. Hess, H. Prinz, A. Zychlinsky, H. Waldmann, Activation of the Raf-MEK-ERK pathway is required for neutrophil extracellular trap formation, Nat. Chem. Biol. 7 (2011) 75–77.
[14] C. Schorn, C. Janko, V. Krenn, Y. Zhao, L.E. Munoz, G. Schett, M. Herrmann, Bonding the foe – NETting neutrophils immobilize the pro-inflammatory monosodium urate crystals, Front. Immunol. 3 (2012) 376.
[15] H. Parker, M. Dragunow, M.B. Hampton, A.J. Kettle, C.C. Winterbourn, Requirements for NADPH oxidase and myeloperoxidase in neutrophil extracellular trap formation differ depending on the stimulus, J. Leukocyte Biol. 92 (2012) 841–849.
[16] F.H. Pilsczek, D. Salina, K.K. Poon, C. Fahey, B.G. Yipp, C.D. Sibley, S.M. Robbins, F.H. Green, M.G. Surette, M. Sugai, M.G. Bowden, M. Hussain, K. Zhang, P. Kubes, A novel mechanism of rapid nuclear neutrophil extracellular trap formation in response to Staphylococcus aureus, J. Immunol. 185 (2010) 7413–7425.
[17] A.S. Byrd, X.M. O'Brien, C.M. Johnson, L.M. Lavigne, J.S. Reichner, An extracellular matrix-based mechanism of rapid neutrophil extracellular trap formation in response to Candida albicans, J. Immunol. 190 (2013) 4136–4148.
[18] V. Brinkmann, A. Zychlinsky, Neutrophil extracellular traps: is immunity the second function of chromatin?, J Cell Biol. 198 (2012) 773–783.
[19] A.K. Gupta, P. Hasler, W. Holzgreve, S. Gebhardt, S. Hahn, Induction of neutrophil extracellular DNA lattices by placental microparticles and IL-8 and their presence in preeclampsia, Hum. Immunol. 66 (2005) 1146–1154.
[20] R. Manzenreiter, F. Kienberger, V. Marcos, K. Schilcher, W.D. Krautgartner, A. Obermayer, M. Huml, W. Stoiber, A. Hector, M. Griese, M. Hannig, M. Studnicka, L. Vitkov, D. Hartl, Ultrastructural characterization of cystic fibrosis sputum using atomic force and scanning electron microscopy, J. Cyst. Fibros. 11 (2012) 84–92.
[21] A. Hakkim, B.G. Furnrohr, K. Amann, B. Laube, U.A. Abed, V. Brinkmann, M. Herrmann, R.E. Voll, A. Zychlinsky, Impairment of neutrophil extracellular trap degradation is associated with lupus nephritis, Proc. Natl. Acad. Sci. U.S.A. 107 (2010) 9813–9818.
[22] J. Xu, X. Zhang, R. Pelayo, M. Monestier, C.T. Ammollo, F. Semeraro, F.B. Taylor, N.L. Esmon, F. Lupu, C.T. Esmon, Extracellular histones are major mediators of death in sepsis, Nat. Med. 15 (2009) 1318–1321.
[23] A.K. Gupta, M.B. Joshi, M. Philippova, P. Erne, P. Hasler, S. Hahn, T.J. Resink, Activated endothelial cells induce neutrophil extracellular traps and are susceptible to NETosis-mediated cell death, FEBS Lett. 584 (2010) 3193–3197.
[24] D.I. Feig, D.H. Kang, R.J. Johnson, Uric acid and cardiovascular risk, N. Engl. J. Med. 359 (2008) 1811–1821.
[25] N.L. Edwards, The role of hyperuricemia in vascular disorders, Curr. Opin. Rheumatol. 21 (2009) 132–137.

Please cite this article in press as: Y. Arai et al., Uric acid induces NADPH oxidase-independent neutrophil extracellular trap formation, Biochem. Biophys. Res. Commun. (2013), http://dx.doi.org/10.1016/j.bbrc.2013.12.007

OPEN ACCESS Freely available online

PLOS ONE

CKIP-1 Is an Intrinsic Negative Regulator of T-Cell Activation through an Interaction with CARMA1

Takashi Sakamoto[1], Masayuki Kobayashi[1]*, Kohei Tada[1], Masanobu Shinohara[1], Katsuhiro Io[1], Kayoko Nagata[1], Fumie Iwai[1], Yoko Takiuchi[1], Yasuyuki Arai[1], Kouhei Yamashita[1], Keisuke Shindo[1], Norimitsu Kadowaki[1], Yoshio Koyanagi[2], Akifumi Takaori-Kondo[1]

1 Department of Hematology and Oncology, Graduate School of Medicine, Kyoto University, Kyoto, Japan, **2** Laboratory of Viral Pathogenesis, Institute for Virus Research, Kyoto University, Kyoto, Japan

Abstract

The transcription factor NF-κB plays a key regulatory role in lymphocyte activation and generation of immune response. Stimulation of T cell receptor (TCR) induces phosphorylation of CARMA1 by PKCθ, resulting in formation of CARMA1-Bcl10-MALT1 (CBM) complex at lipid rafts and subsequently leading to NF-κB activation. While many molecular events leading to NF-κB activation have been reported, it is less understood how this activation is negatively regulated. We performed a cell-based screening for negative regulators of TCR-mediated NF-κB activation, using mutagenesis and complementation cloning strategies. Here we show that casein kinase-2 interacting protein-1 (CKIP-1) suppresses PKCθ-CBM-NF-κB signaling. We found that CKIP-1 interacts with CARMA1 and competes with PKCθ for association. We further confirmed that a PH domain of CKIP-1 is required for association with CARMA1 and its inhibitory effect. CKIP-1 represses NF-κB activity in unstimulated cells, and inhibits NF-κB activation induced by stimulation with PMA or constitutively active PKCθ, but not by stimulation with TNFα. Interestingly, CKIP-1 does not inhibit NF-κB activation induced by CD3/CD28 costimulation, which caused dissociation of CKIP-1 from lipid rafts. These data suggest that CKIP-1 contributes maintenance of a resting state on NF-κB activity or prevents T cells from being activated by inadequate signaling. In conclusion, we demonstrate that CKIP-1 interacts with CARMA1 and has an inhibitory effect on PKCθ-CBM-NF-κB signaling.

Citation: Sakamoto T, Kobayashi M, Tada K, Shinohara M, Io K, et al. (2014) CKIP-1 Is an Intrinsic Negative Regulator of T-Cell Activation through an Interaction with CARMA1. PLoS ONE 9(1): e85762. doi:10.1371/journal.pone.0085762

Editor: Kjetil Tasken, University of Oslo, Norway

Received September 16, 2013; **Accepted** December 5, 2013; **Published** January 17, 2014

Funding: This work was supported by JSPS KAKENHI Grant Number 23591383. The URL is http://www.jsps.go.jp/j-grantsinaid/. The funders had no role in study design, data collection and analysis, decision to publish, or preparation of the manuscript.

Competing Interests: The authors have declared that no competing interests exist.

* E-mail: mkobayas@kuhp.kyoto-u.ac.jp

Introduction

The NF-κB family of transcription factors plays a key regulatory role in lymphocyte activation and generation of immune response [1]. The respective NF-κB target genes allow the organism to respond effectively to the environmental changes. Engagement of TCR by specific antigen presented on major histocompatibility complex (MHC) of antigen presenting cells (APC) induces T cell activation and proliferation. However, stimulation of TCR/CD3 complex alone is not sufficient for activation of NF-κB. The simultaneous costimulation of CD28 through its ligand, B7, is needed for optimal activation of NF-κB [2]. CD3/CD28 costimulation induces the formation of a large multicomponent complex at the contact site between T cell and the APC, termed as immunological synapse [3,4]. This contact area of T cells is highly enriched in cholesterol and glycosphingo-lipids, also termed as lipid rafts, and serve as the platform for the assembly of proximal signaling components of TCR. PKCθ is recruited to the immunological synapse from the cytosol upon T cell stimulation and catalytically activated [5,6]. Activated PKCθ phosphorylates CARMA1 (CARD11) to induce its conformational changes which enable CARMA1 to form the complex with Bcl10-MALT1 [7,8]. Subsequently, the IκB kinase (IKK) complex becomes activated and phosphorylates IκBs, leading to their ubiquitylation and subsequent proteasomal degradation. The degradation of IκBs allows NF-κB to enter the nucleus and induce transcription of target genes [1].

CARMA1 is one of a family of caspase recruitment domain (CARD)- and membrane associated guanylate kinase-like (MAGUK) domain-containing proteins (CARMA) [9,10]. CARMA1 contains an N-terminal CARD, followed by a coiled-coil (CC) domain, a PDZ domain, a Src homology 3 (SH3) domain, and a guanylate kinase (GUK)-like domain in the C-terminus. It has two mammalian homologs, CARMA2 and CARMA3. CARMA1 is predominantly expressed in spleen, thymus, and peripheral blood leukocyte (PBL); CARMA2 is expressed only in placenta; and CARMA3 is expressed in broad range of tissues but not in spleen, thymus or PBL. For B and T cells, the scaffold protein CARMA1 plays an essential role in antigen receptor-induced NF-κB activation [11–15]. Aberrant NF-κB activation could be involved in autoimmune diseases and malignant lymphomas. Constitutively active NF-κB in the activated B cell-like (ABC) subtype of diffuse large B cell lymphoma (DLBCL) can result from somatic mutations in genes involved in NF-κB signaling, such as CD79B, A20 and CARMA1 [16]. Recently, germline mutations in CARMA1 have also been reported in four patients with congenital B cell lymphocytosis [17]. Therefore CARMA1 activity needs to be tightly regulated.

Casein kinase-2 interacting protein-1 (CKIP-1) was originally identified as an interacting protein of casein kinase 2α (CK2α) [18]. CKIP-1 contains a pleckstrin homology (PH) domain at the N-terminus, a leucin zipper (LZ) motif at the C-terminus, and five proline-rich motifs throughout the protein [19]. Several interacting proteins of CKIP-1 have been identified and CKIP-1 plays scaffold roles in various signaling pathways [18–27]. It has also been reported that CKIP-1 binds to lipid through its PH domain and contributes to localization of its binding proteins. Genetically, CKIP-1-deficient mice show an age-dependent increase in bone mass as a result of accelerated osteogenesis, and the MEKK2-JNK-c-Jun/AP-1 axis is activated in CKIP-1 deficient mouse embryonic fibroblasts [22,25]. However, the role of CKIP-1 in NF-κB signaling remains unknown.

Many findings leading to NF-κB activation have been reported, but it is less understood how this activation is negatively regulated. To elucidate negative regulation in TCR-mediated NF-κB activation, we have done a screening by mutagenesis and complementation cloning strategies. Here we report the identification of CKIP-1 as a negative regulator in NF-κB signaling via TCR. We show that CKIP-1 interacts with CARMA1, inhibits the interaction between PKCθ and CARMA1, and suppresses NF-κB activation.

Materials and Methods

Cells

CARMA1-deficient Jurkat T cell line, named JPM50.6, and JPM50.6/WT cell line, which was reconstituted with Myc-tagged CARMA1 wild type (WT) in JPM50.6, were kindly gifted from Dr. Xin Lin [11,28]. These cell lines and Jurkat T cells were maintained with RPMI1640 (Nacalai Tesque, Kyoto, Japan) containing 10% fetal bovine serum (FBS) and 1% penicillin-streptomycin and glutamine (PSG) (Invitrogen, Carlsbad, USA). HEK293T cells were maintained with DMEM (Nacalai Tesque) containing 10% FBS and 1% PSG.

Generation of mutant Jurkat T cells and complementation cloning strategies by lentiviral cDNA library

Jurkat T cell line stably expressing EGFP under the control of an NF-κB-dependent promoter, which we called JR-GFP, was kindly gifted from Dr. Xin Lin [11]. To generate mutant cells, JR-GFP cells were treated with 4 μg/ml of ICR191 (Sigma-Aldrich, St. Louis, USA), alkylating agent that typically generates random frame-shift mutations [11,29], for 5 hr, and this treatment was repeated three times. After mutagenesis, EGFP-positive cells were sorted by BD FACSAria cell sorter (BD, New Jersey, USA) under the treatment with 2.5 μM of PKC inhibitor GF109203X (Sigma-Aldrich). Monoclonal mutant cell lines were derived by limiting dilution, and, among them, an NF-κB constitutively active cell line was identified. Human leukocyte cDNA library (Invitrogen) on pCS2-EF-GATEWAY-IRES-hrGFP was transferred into pCS2-EF-GATEWAY-IRES-H2K^k through LR reaction on Gateway cloning system (Invitrogen) and cDNA and H2K^k-dual expressing lentiviral vector were prepared as described before [30,31]. To identify NF-κB negative regulators, the NF-κB constitutively active cell line was infected with this viral vector. If the mutant phenotype was rescued by the gene from the library, EGFP expression might return to negative. Both H2K^k-positive and EGFP-negative cells were sorted using BD FACSAria cell sorter and subjected to limiting dilution. If EGFP was normally induced by PMA/ionomycin in each single cell clone, the mutant phenotype should be rescued by the gene from the library. The genes rendering the reversion of the mutant phenotype were isolated by PCR using vector specific primers. Subsequent DNA sequencing and BLAST analysis should reveal the integrated gene.

Plasmid constructs

Plasmids encoding Myc-CARMA1, Myc-CARMA1 truncated forms, EGFP-CARMA1, Myc-Bcl10, PKCθ WT, PKCθ AE [32], IKKβ, and GFP-NF-κB RelA were kind gifts from Dr. Xin Lin. Expression vectors for FLAG-CARMA1 and HA-Bcl10 were generated by subcloning of coding sequence into pcDNA3 vector (Invitrogen). GST-CARMA1 CD-CC was generated by subcloning of coding sequence into pGEX-4T-1 (GE Healthcare, Buckinghamshire, UK). Human CKIP-1 cDNA was generated by PCR amplification from Jurkat cDNA and cloned into pcDNA3/hygro and pcDNA3-FLAG vector (Invitrogen). Expression vector for DsRed-CKIP-1 was generated by subcloning of coding sequence into pDsRed1-N1 vector (Clontech, Mountain View, USA). ΔLZ-CKIP-1 and ΔPH-CKIP-1 truncated form were generated by PCR amplification from WT CKIP-1 expression vector and subcloned into pcDNA3/hygro vector.

RNA interference

To identify a negative signaling component of NF-κB signaling from our candidates, we knocked down the molecules by specific siRNA in JR-GFP cells. siRNAs against our selected eighteen candidates were purchased from Thermo Scientific (Rockford, USA) (siGENOME SMARTpool). 5×10^6 JR-GFP cells were electroporated with 400 pmol of non-targeting siRNA (D-001206-13), human TNFAIP3 (A20)-specific siRNA (M-009919-00), human CKIP-1-specific siRNA (M-016800-01), and siRNAs against other seventeen genes using AMAXA Nucleofector System (Lonza, Basel, Switzerland). Five days later, EGFP expression was analyzed by BD FACSCalibur. siRNA SMARTpool (Thermo Scientific) is a mixture of four siRNAs. We also used separate aliquot of four individual siRNAs (D-016800-01, 02, 03, 04).

Chemicals, Cytokines, and Antibodies

PMA and ionomycin were purchased from Sigma-Aldrich. TNFα was from CellGenix (Freiburg, Germany). PE-conjugated anti-mouse H2K^k (CL9005PE) was from Cedarlane (Ontario, Canada). Anti-GFP (A6455) was from Molecular Probes (Eugene, USA). Mouse anti-human CD3 (555336), -CD28 (555725), and -PKCθ (610089) were from BD Biosciences (San Jose, USA). Anti-CKIP-1 (D-20, sc-50225), -IKKα/β (H470, sc-7607), and -Lck (3A5, sc-433) were from Santa Cruz Biotechnology (Santa Cruz, USA). Anti-β-actin (AC-15, A5441), -c-Myc (9E10, M5546, and C3956), and -FLAG (M2, F3165) were from Sigma-Aldrich. Anti-HA (12CA5) was from Roche (Mannheim, Germany). Anti-p-Erk (Thr202/Tyr204, E10, #9106), -Erk (#9102), and -CARMA1 (1D12, #4435) were from Cell Signaling Technology (Danvers, USA).

Luciferase reporter assay

5 μg of 5xNF-κB-dependent luciferase (*Firefly*) reporter plasmid and 0.1 μg of EF1α promoter-dependent *Renilla* luciferase reporter were transfected together with 5 μg of plasmids encoding the desired genes or 400 pmol of siRNA by electroporation into 1×10^7 Jurkat T cells in 0.4 ml serum-free RPMI1640 media at the power setting of 250 V and 950 μF. Nineteen hours later, the transfected cells were treated for 5 hr with plate-bound CD3 mAb (2 μg/ml), plate-bound CD3 + soluble CD28 mAb (2 μg/ml of each), TNFα (20 ng/ml), PMA (10 ng/ml), or PMA (10 ng/ml) + CD28 (2 μg/ml). NF-κB activity was measured with Dual-

Luciferase Reporter Assay System (Promega, Madison, USA) and was determined by normalization of NF-κB-dependent *Firefly* luciferase to *Renilla* luciferase activity. Values represent the average of three independent experiments and error bars represent the SD from the average. Statistically significance was determined using Student's t test.

Evaluation of NF-κB activity

Nuclear protein fractions were harvested by the Nuclear Extract kit (Active Motif, Carlsbad, USA). NF-κB activity was measured in 2 μg of nuclear protein extracts by the TransAM™ NF-κB p65 chemi (Active Motif), an ELISA-based kit to detect and quantify NF-κB p65 subunit activation. The assay was performed according to the manufacturer's protocol and analyzed using a microplate luminometer PerkinElmer 2030 ARVO™ X3 (PerkinElmer, Waltham, USA). Values represent the average of three independent experiments and error bars represent the SD from the average. Statistically significance was determined using Student's t test.

Immunoprecipitation

For co-immunoprecipitation, 6-well plate HEK293T cells were transfected by the calcium phosphate method. Two days after transfection, cells were lysed in NP-40 lysis buffer (20 mM Tris-HCl pH 7.5, 250 mM NaCl, 1% NP-40) supplemented with 1 mM PMSF, protease inhibitor cocktail (Nacalai Tesque) and phosphatase inhibitor cocktail (Roche). Total cell lysates were precleared on Protein A Sepharose beads for 30 min at 4°C. The precleared cell lysates were immunoprecipitated with Protein A beads-conjugated with the desired antibodies for 6 hr. Immunoprecipitates were washed three times with lysis buffer.

To detect the protein interaction in JPM50.6/WT cells, 1×10^8 cells were lysed in NP-40 lysis buffer (10 mM Tris-HCl pH 7.5, 150 mM NaCl, 0.5% NP-40) supplemented with protease inhibitor cocktail (Nacalai Tesque) and phosphatase inhibitor cocktail (Roche). Total cell lysates were precleared on Protein A Sepharose beads for 30 min at 4°C. The precleared cell lysates were immunoprecipitated with Protein A beads-conjugated with 2 μg of anti-CKIP-1 Ab at 4°C overnight. Immunoprecipitates were washed three times with 0.05% NP-40 buffer (10 mM Tris-HCl pH 7.5, 150 mM NaCl, 0.05% NP-40).

Confocal microscopy

HEK293T cells were transfected with expression vectors and grown on the coverslips. 24 hr after transfection, the cells were incubated with Alexa Flour 488-conjugated cholera toxin B (Molecular probes) at 4°C for 20 min. The specimens were fixed with 4% paraformaldehyde in PBS and mounted on slides using ProLong Gold antifade reagent with DAPI (Invitrogen), and analyzed by confocal laser scanning fluorescence microscopy (Nikon Digital Eclipse C1).

In vitro binding assay

FLAG-CKIP-1 was synthesized *in vitro* using the TNT T7 Quick Coupled Transcription/Translation System (Promega). GST and GST-CARMA1 CD-CC proteins were produced in *E. coli* BL21 and purified with glutathione Sepharose 4B beads (GE Healthcare). The beads were incubated with FLAG-CKIP-1 at 4°C for 2 hr. The beads were washed and proteins were eluted, followed by Western blotting with anti-FLAG antibody.

Lipid raft purification

Costimulation of Jurkat T cells was performed in a final volume of 1 ml by addition of anti-CD3 (10 μg/ml) and anti-CD28 (5 μg/ml) antibodies, together with 15 μg of mouse IgG (Sigma-Aldrich). Cells (2×10^7) were lysed in 1 ml MNE Buffer (25 mM MES pH 6.5, 150 mM NaCl, 5 mM EDTA) with 1% Triton-X, 1 mM PMSF, and protease inhibitor cocktail (Nacalai Tesque) for 20 min on ice and dounce homogenized 20 times. Samples were centrifuged at 1,000× g for 10 min at 4°C. The supernatants were mixed with 1 ml of OptiPrep (Axis-Shield, Oslo, Norway) and transferred to a Beckman Ultracentrifuge tube. Two milliliters of 30% OptiPrep followed by 1 ml of 5% OptiPrep in MNE buffer were overlaid. Samples were ultracentrifuged in a SW41Ti rotor (200,000× g for 20 hr). Fractions (400 μl per fraction) were collected from the top of the gradient. Proteins from each fraction were precipitated with trichloroacetic acid before separation by SDS-PAGE and Western blotting.

Results

Identification of CKIP-1 as a negative regulator of NF-κB activation

We have performed a cell-based screening to find negative regulators in TCR-mediated NF-κB activation, using somatic mutagenesis and complementation cloning strategies [11,29]. We used Jurkat T cell line expressing EGFP under the control of an NF-κB-dependent promoter, named JR-GFP [11]. To generate NF-κB constitutively active cell lines, JR-GFP cells were subjected to mutagenesis with ICR191, and EGFP-positive cells were sorted under the treatment of PKC inhibitor GF109203X. After limiting dilution, we identified an NF-κB constitutively active cell line in which negative regulators for NF-κB activation must be mutated. To identify NF-κB negative regulators, the NF-κB constitutively active cell line was infected with a human leukocyte-cDNA library expressing lentivirus, and EGFP-negative cells were sorted. If the mutant phenotype was rescued by transduction of the gene from the library, EGFP expression would return to negative. The genes rendering the reversion of the mutant phenotype were isolated by PCR and sequenced using library vector specific primers, and then we obtained dozens of candidates for NF-κB negative regulators. To examine whether any of these candidates downregulate NF-κB activity, we selected and knocked down eighteen molecules by specific siRNA in JR-GFP cells. We found that knockdown of CKIP-1 induced expression of EGFP more than that of TNFAIP3 (A20), which was known as a negative regulator of NF-κB and used as a positive control [33] (Figure S1). To confirm that CKIP-1 was a negative regulator of NF-κB, Jurkat T cells were transfected with CKIP-1 siRNA together with an NF-κB-dependent luciferase reporter plasmid. We used siRNA SMARTpool, which is a mixture of four siRNAs, and separate aliquot of all four individual siRNAs. Knockdown of CKIP-1 increased NF-κB activity (Figure 1A). We also showed that knockdown of CKIP-1 induced DNA binding activity of NF-κB p65 (Figure 1B), by using the transcription factor DNA-binding ELISA. Thus, we clearly demonstrated that CKIP-1 was a novel NF-κB negative regulator.

CKIP-1 suppresses NF-κB activation induced by PMA and constitutively active PKCθ

To examine whether the downregulation of NF-κB activation by CKIP-1 is specific to TCR stimulation, Jurkat T cells transfected with CKIP-1, treated with different stimulation, and assessed NF-κB activity by luciferase reporter assays. CKIP-1 suppressed NF-κB activity in unstimulated cells and stimulated by CD3, PMA and PMA/CD28, but not by TNFα or CD3/CD28

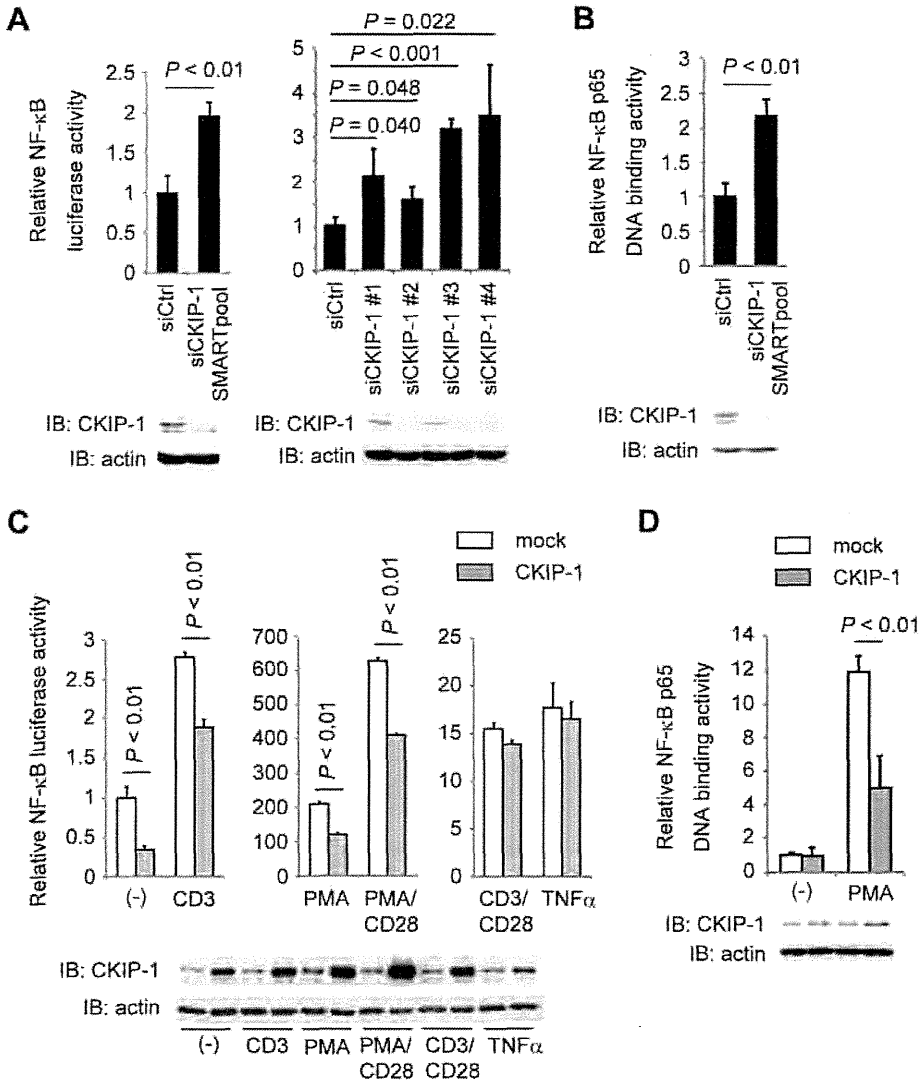

Figure 1. Identification of CKIP-1 as a negative regulator in NF-κB activation. (A) 400 pmol of human CKIP-1-specific siRNA or non-targeting siRNA together with 5 μg of κB-Luc, 0.1 μg of *Renilla*-Luc were electroporated into Jurkat T cells. Luciferase activity was assayed after 48 hr. The reduction of endogenous CKIP-1 protein levels was analyzed by Western blotting. (B) Jurkat T cells were electroporated with human CKIP-1-specific siRNA or non-targeting siRNA using AMAXA Nucleofector System (Lonza). Thirty hours later, nuclear protein extracts were harvested and NF-κB activity was measured by TransAM NF-κB p65 chemi kit (Active Motif). The reduction of endogenous CKIP-1 protein levels was analyzed by Western blotting. (C) Jurkat T cells were transfected with 5 μg of CKIP-1 or empty vector (mock) together with 5 μg of κB-Luc and 0.1 μg of *Renilla*-Luc. Nineteen hours later, cells were stimulated for 5 hr upon CD3 (2 μg/ml), CD3/CD28 (2 μg/ml each), TNFα (20 ng/ml), PMA (10 ng/ml) or PMA (10 ng/ml) + CD28 (2 μg/ml). The expressed protein levels were analyzed by Western blotting. (D) Jurkat T cells were transfected with 5 μg of CKIP-1 or empty vector (mock). Twenty-four hours later, cells were stimulated for 30 min upon PMA (10 ng/ml). Then cells were harvested and NF-κB activity was measured by TransAM NF-κB p65 chemi kit. The expressed protein levels were analyzed by Western blotting. Values represent the average of three independent experiments and error bars represent the SD from the average.
doi:10.1371/journal.pone.0085762.g001

(Figure 1C). Using the transcription factor DNA-binding ELISA, we also showed that CKIP-1 suppressed NF-κB activation induced by PMA stimulation (Figure 1D). These data suggest that CKIP-1 inhibits NF-κB signaling via TCR but not via TNF receptor and that CKIP-1 targets downstream signaling components of PKCθ, since the treatment of PMA directly activates PKCs. To clarify which step of signaling CKIP-1 affects, NF-κB activation driven by transfection of each downstream signaling component of PKCθ was assessed in Jurkat T cells in the presence or absence of co-transfection of CKIP-1 (Figure 2A). NF-κB activation induced by PKCθ AE, a constitutively active mutant [32], was clearly suppressed by CKIP-1, whereas activation induced by NF-κB RelA, IKKβ or Bcl10 was not affected. NF-κB activation induced by CARMA1 seemed to be suppressed by CKIP-1, but the effect was not statistically significant. Conversely, knockdown of CKIP-1 increased NF-κB activation induced by transfection of CARMA1 or PKCθ AE (Figure 2B). These results suggest that the inhibitory effect of CKIP-1 targets signaling events around PKCθ or CARMA1.

As shown in Figure 1C, CKIP-1 did not suppress CD3/CD28-induced NF-κB activation. We hypothesized that CKIP-1 might work in a resting state and finish its role during CD3/CD28 costimulation. PKCθ and CARMA1 have been reported to be recruited to lipid rafts upon TCR stimulation [34]. It has been

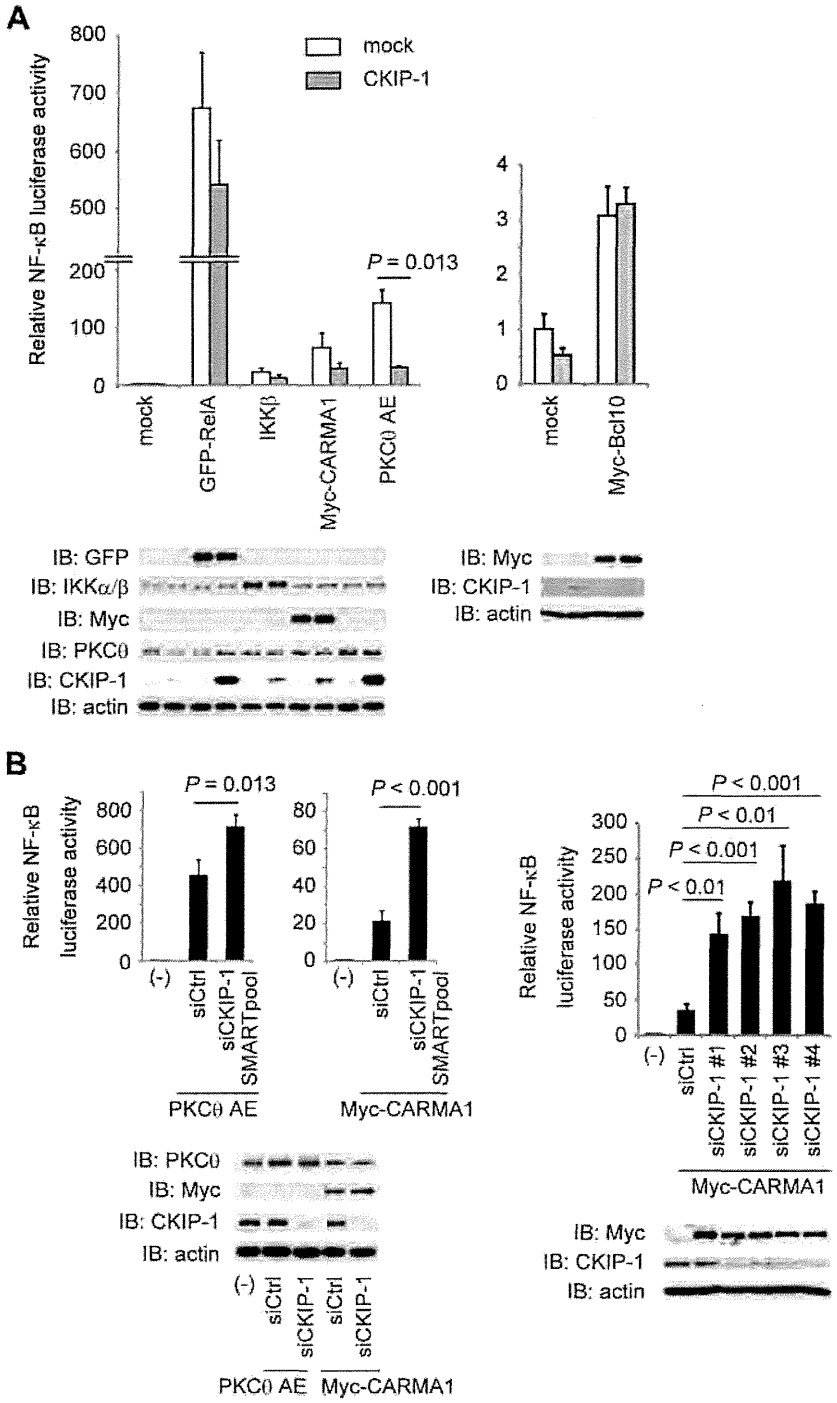

Figure 2. CKIP-1 suppresses NF-κB activation induced by constitutively active PKCθ. (A) Jurkat T cells were transfected with 5 μg of CKIP-1 or empty vector (mock) together with 5 μg of each signaling component, 5 μg of κB-Luc and 0.1 μg of *Renilla*-Luc by electroporation. Luciferase activity was assayed after 24 hr. PKCθ AE is constitutively active mutant. The expressed protein levels were analyzed by Western blotting. (B) Jurkat T cells were transfected with 400 pmol of human CKIP-1-specific siRNA or non-targeting siRNA together with 5 μg of κB-Luc, 0.1 μg of *Renilla*-Luc, and 5 μg of PKCθ AE (left panel) or CARMA1 (right panel) by electroporation. Thirty hours later, cells were lysed and luciferase activity was assayed. The expressed protein levels were analyzed by Western blotting. Values represent the average of three independent experiments and error bars represent the SD from the average.
doi:10.1371/journal.pone.0085762.g002

shown that CKIP-1 binds to lipid through its PH domain and overexpressed CKIP-1 localizes in the plasma membrane and partly in the nucleus [18,20,22]. To examine where CKIP-1 localizes in Jurkat T cells, the detergent-insoluble membrane (lipid raft) fractions were prepared by the ultra-centrifugation in a discontinuous OptiPrep density gradient. Lck was constitutively associated with lipid rafts, and PKCθ was recruited to lipid rafts after CD3/CD28 costimulation (Figure 3) as previously reported